Master Thesis

# The axial charge of the Λ-baryon from Lattice QCD

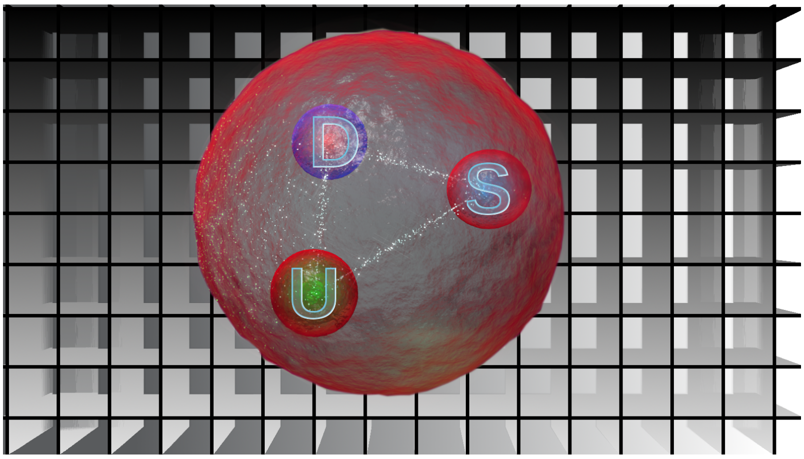


**Masterarbeit in Physik**
**vorgelegt dem Fachbereich Physik, Mathematik und Informatik**
**(FB 08)**
**der Johannes Gutenberg-Universität Mainz**
**am 16. Februar 2016**

von

**Yilmaz Ayten**

1. Gutachter: Prof. Dr. Hartmut Wittig
2. Gutachter: PD Dr. Georg von Hippel

Ich versichere, dass ich die Arbeit selbstständig verfasst und keine anderen als die angegebenen Quellen und Hilfsmittel benutzt sowie Zitate kenntlich gemacht habe.

Mainz, den 16.02.2015______________________
*Unterschrift*

Yilmaz Ayten
Institut für Kernphysik
Johann-Joachim-Becher-Weg 45
Johannes Gutenberg-Universität D-55099 Mainz
ayten@mail.kph.uni-mainz.de

# Abstract

Lattice Quantum chromodynamics (LQCD) has grown to a reliable tool to study hadronic quantities at low energy. One of these quantities is the axial charge $g_A$. The axial charge of the nucleon is a ideal benchmark quantity, since there exist a experimental value. In thesis though the axial charge of the $\Lambda$ baryon is calculated, for which experimental value remains. Extracting the axial charge requires the evaluation of two- and three-point functions. These functions are calculated by using the quark propagators, which results from the inversion of a large matrix.

# Zusammenfassung

Die "Gitter-Quantenchromodynamik" is zu einer verlässlichen Theorie gewachsen, um die Eigenschaften der Hadronen bei niedrigen Energien zu untersuchen. Die axiale Ladung $g_A$ des Nukleons ist eine ideale Bezugswertsgröße, da experimentelle Werte existieren. In der vorliegenden Arbeit wird die axiale Ladung des $\Lambda$ Baryons berechnet, für die die experimentelle Bestimmung noch aussteht. Die Bestimmung der axialen Ladung erfordert die Berechnung von Zwei- und Dreipunktsfunktionen. Diese Funktionen werden durch Quarkpropagatoren bestimmt, die durch die Inversion großer Matrizen entstehen.

# Contents


**Introduction** **1**

**1 The strong interaction in continuum and on the lattice** **3**
1.1 Quarks . . . 3
1.2 Gluons and non abelian behaviour . . . 4
1.3 Correlation functions and perturbative quantum field theory . . . 7
1.4 The running coupling $\alpha_s$ . . . 8
1.5 QCD on the Lattice . . . 9
1.6 Discretization of action . . . 10
1.6.1 Fermion doubling and Wilson fermions . . . 12
1.6.2 $\mathcal{O}$(a)-improvement . . . 15
1.7 Requirements for computable path integrals . . . 15
1.7.1 Fermionic expectation value . . . 16
1.7.2 Gluonic expectation value . . . 18
1.8 Scale setting . . . 19
1.9 Lattice set-up . . . 20

**2 Numerical Calculation and the axial charge** **21**
2.1 Propagator . . . 21
2.2 Smearing . . . 22
2.3 Correlator . . . 23
2.4 Time evolution in Euclidean time . . . 25
2.5 The Effective Mass . . . 26
2.6 The axial charge . . . 27
2.6.1 The issue of spin . . . 28
2.7 Calculation of the axial charge of Λ: A theoretical approach . . . 29
2.8 Calculation of axial charge of Λ on the lattice . . . 31
2.8.1 Axial charge: Two-point correlator . . . 31
2.8.2 Axial charge: Three-point correlator . . . 33

**3 Error estimation** **36**
3.1 Jackknife . . . 36
3.2 Signal-to-noise ratio . . . 38

**4 Calculation on the Lattice** **40**
4.1 Λ Two-point correlator . . . 40
4.2 Λ Three-point correlator . . . 44
4.3 Results . . . 48
4.3.1 Summation method . . . 49

**5 Results at the physical point** **52**
5.1 Physical point: Mass . . . 52
5.2 Physical point: Axial charge . . . 54

**6 Summary and outlook** **57**

**A Appendices** **58**
A.1 Gamma matrices . . . . . 58
A.2 Gell-Mann matrices . . . . . 58
A.3 Three-point contraction for u- and d-insertion . . . . . 58
A.3.1 U-insertion . . . . . 58
A.3.2 D-insertion . . . . . 60
A.4 Effective mass plots . . . . . 61

# Introduction

Physicists have succeeded in reducing the fundamental interactions to four basic interactions: The gravitational, electromagnetic, strong and weak interactions. While gravity is governed by Einstein's general relativity, the so-called *Standard Model* describes, by means of *quantum field theory*, the electromagnetic, weak and strong interactions in terms of elementary particles. Particles, which make up "ordinary matter" are called *fermions*, whereas "force mediating" particles are referred to as *bosons*. The unification of the electromagnetic and weak interactions [2, 3, 4] followed by the development of the Higgs mechanism [5], which explains the nonzero mass of the bosons of the weak interactions, leads to the current version of the Standard Model.

In this thesis we focus on the strong interaction described by *quantum chromodynamics (QCD)*, which is the respective quantum field theory. Two types of particles are described in QCD, the quarks and the gluons. The quarks are massive fermions and gluons are the massless bosons of QCD. Quarks and gluons have never been observed as free particles; this phenomenon is called *confinement*. Instead we only observe bound states, the hadrons. Nevertheless, the structure of hadrons, which can be determined by deep inelastic scattering experiments, reveals insight into the interaction of quarks and gluons. There are two members of the hadron particle family: baryons, made of three valence quarks and mesons, made of one quark and one antiquark [6]. Detailed introductions to the theory of strong interaction can be found in [7, 8].

In 1935, Yukawa proposed a force between a member of the baryons, the nucleons, the only baryons which were known at this time. He suggested that the force is mediated by meson exchange [9]. Several more mesons and baryons were discovered later. The axial charge refers to the coupling constant $g_A$ of baryons to mesons, it determines the coupling strength of the baryon-meson interaction. Here we calculate the axial charge of the $\Lambda$-baryon.

The axial charge is a parameter for low-energy effective theories. Unlike quantum electrodynamics, the theory the of electromagnetic interaction, QCD cannot be treated perturbative at low-energy . With low energy we mean the domain $\mu \lesssim 1\,\text{GeV}$, where $\mu$ is identified as the energy scale at which the axial charge is probed [10]. There are two commonly used methods, that have proved to be succesful to study QCD at low energy: *Chiral perturbation theory (ChPT)* [11] and *Lattice QCD* [12]. We will use the method of Lattice QCD to calculate our desired observables.

# 1 The strong interaction in continuum and on the lattice

This section provides a short introduction to QCD in the continuum and on the lattice. We will look at the ingredients of QCD, the quarks and gluons. With these ingredients we will derive the underlying action and show that QCD is non-abelian (non-commutative). We motivate the necessity of the discretized version of QCD and show how this affects the whole theory. General introductions can be found in [7, 8] for continuum QCD and in [13, 14] for lattice QCD.

## 1.1 Quarks

The matter fields of QCD are called quarks. They show up in 6 different flavors $f$, up($u$), down($d$), charm($c$), strange($s$), top($t$) and bottom($b$) and are distinguished by their mass and associated quantum numbers. We distinguish between two kinds of quarks; the light ones and the heavy ones. In Table 1 all properties are summarized.

| | | | |
|---|---|---|---|
| **light Quarks** | | | |
| Flavor | u | d | s |
| Mass[Mev] | $2.3^{+0.7}_{-0.5}$ | $4.8^{+0.5}_{-0.3}$ | $95 \pm 5$ |
| Charge[e] | $\frac{2}{3}$ | $-\frac{1}{3}$ | $-\frac{1}{3}$ |
| Quantum number | $I_Z = \frac{1}{2}$ | $I_Z = -\frac{1}{2}$ | strangeness=-1 |
| **heavy Quarks** | | | |
| Flavor | c | b | t |
| Mass[Mev] | $1.275 \pm 0.025$ | $4.18 \pm 0.03$ | $173.5 \pm 0.6$ |
| Charge[e] | $\frac{2}{3}$ | $-\frac{1}{3}$ | $\frac{2}{3}$ |
| Quantum number | charm=+1 | bottomness=-1 | topness=+1 |

**Table 1:** Here $I_Z$ denotes the isospin z-component. The values are determined from PDG [6, 15]

Quarks are affected by the strong interaction, as they carry *color charges* $c$. Unlike the electrical charge, the color charge is not additive. It is a charge in the sense that the combination of quarks follows group theoretical rules like the combinations of angular momenta in quantum mechanics [7]. There are three color charges $c$= {red, green and blue} or {1, 2, 3}. Quarks are spin-1/2 particles, ergo fermions, and we assume that they are point-like objects. To describe quarks, we define a mathematical object called field, that is defined by their values $\psi(x)$ at every point in space and time $x$. We denote fermions and antifermions by Dirac 4-spinors $\psi^{(f)}(x)_{\alpha c}$ and $\overline{\psi}^{(f)}(x)_{\alpha c}$ with the Dirac index $\alpha$ ={1, 2, 3, 4}. Isolated color charges have so far not been observed. This phenomenon is known as *color confinement*. A fully theoretical description of this phenomenon though is not developed [16]. Free quarks, i.e. no interacting quarks, obey the free Dirac equation

$$\left(i\gamma_\mu\partial^\mu - m\right)\psi(x) = 0, \tag{1}$$

with $\gamma_\mu$ the Dirac matrices which are defined in appendix A.1 and $m$ the free mass. Here we use the Einstein summation convention and a matrix/vector notation for the color and Dirac indices. The free Dirac equation can be obtained from the Lagrangian density

$$\mathscr{L}_{\text{free}}(x) = \overline{\psi}(x)\left(i\gamma_\mu\partial^\mu - m\right)\psi(x). \tag{2}$$

We demand, that QCD is invariant under a local[1] color transformation, i.e., the Lagrangian density should be invariant under a transformation $\Omega(x)$. The group element $\Omega(x)$ of SU(3) can be build with the associated 8 generators $\frac{\lambda^a}{2}$ ($a = \{1,\ldots,8\}$), the *Gell-Mann matrices* $\lambda_a$ (see appendix A.2). The spinors transform as

$$\begin{aligned}\psi(x) &\longrightarrow \psi'(x) = \exp\left(i\theta_a(x)\frac{\lambda^a}{2}\right)\psi(x) = \Omega(x)\psi(x),\\ \overline{\psi}(x) &\longrightarrow \overline{\psi}(x)\Omega^\dagger(x),\end{aligned} \tag{3}$$

where $\theta_a$ are real parameters. Inserting the transformed spinors into the free lagrangian density we get

$$\mathscr{L}_{\text{free}}(x) \longrightarrow \mathscr{L}'_{\text{free}}(x) = \mathscr{L}_{\text{free}}(x) - i\psi(x)\gamma_\mu\left(\partial^\mu\Omega(x)\right)\psi(x). \tag{4}$$

We see that the free Lagrangian is not invariant under local SU(3)-transformations: The derivative in the kinetic term breaks the symmetry. To fix this, we introduce a gauge field.

## 1.2 Gluons and non abelian behaviour

Gluons are the bosons of QCD, they also carry a color charge. They have no electrical charge and are massless. The color charge is compound of a "color" and an "anti color". Gluons couple with the quarks and the interaction of quark and quark are mediated by them. Due to the color symmetry, there are 8 types of gluons. The gauge field $A_\mu$ (in QCD they are understood as gluons) is defined as

$$A^\mu(x) = \sum_{a=1}^{8} A_a^\mu \frac{\lambda^a}{2}, \tag{5}$$

[1] the transformation is $x$ dependent

with real-valued fields $A_a^\mu$. Returning to the free Lagrangian in eq. (2): The derivative loses its meaning when applying the transformation defined in eq. (3). This can be seen if we consider the derivative along the direction $n^\nu$

$$n^\mu \partial_\mu \psi(x) = \lim_{\epsilon \longrightarrow 0} \frac{\psi(x+\epsilon\hat{n}) - \psi(x)}{\epsilon}. \tag{6}$$

Applying the transformation for spinors (eq. 3), we see that $\psi(x+\epsilon\hat{n})$ and $\psi(x)$ transform differently. $\psi(x+\epsilon\hat{n})$ transforms with $\Omega(x+\epsilon\hat{n})$ and $\psi(x)$ with $\Omega(x)$. Thus, the derivative $\partial_\mu \psi(x)$ has no simple transformation law and we cannot compare $\psi(x)$ at different points. To fix the derivative, we have to introduce the so-called *covariant derivative* $D_\mu$ which transforms as

$$D_\mu \psi(x) \longrightarrow D_\mu \psi'(x) = \Omega(x) D_\mu \psi(x). \tag{7}$$

To find such a derivative we define an object $U(y,x)$, which depends on two points and transforms as

$$U(y,x) \longrightarrow U'(y,x) = \Omega(y) U(y,x) \Omega^\dagger(x). \tag{8}$$

Applying $U(y,x)$ the transformation of $\psi(x)$ is equal to that of $\psi(y)$ , i.e

$$U(y,x)\psi(x) \longrightarrow \Omega(y) U(y,x) \underbrace{\Omega^\dagger(x)\Omega(x)}_{=\mathbb{1},\text{ since }\Omega\in SU(3)} \psi = \Omega(y)\big(U(y,x)\psi(x)\big). \tag{9}$$

$U(y,x)$ "transports" the gauge transformation from $x$ to $y$. With $U(y,x)$ we can build a difference at two points with the same transformation properties. Taking $y = x + \epsilon\hat{n}$, $D_\mu$ can be defined as

$$n^\mu D_\mu \psi(x) = \lim_{\epsilon \longrightarrow 0} \frac{\psi(x+\epsilon\hat{n}) - U(x+\epsilon\hat{n}, x)\psi(x)}{\epsilon}. \tag{10}$$

Thus $D_\mu$ transforms as

$$D_\mu \psi(x) \longrightarrow \lim_{\epsilon \longrightarrow 0} \Omega(x+\epsilon\hat{n}) D_\mu \psi(x) = \Omega(x) D_\mu \psi(x), \tag{11}$$

and from this we see that the Lagrangian

$$\mathscr{L}_q = \overline{\psi}(x)\big(i\gamma_\mu D^\mu - m\big)\psi(x) \tag{12}$$

is invariant. To construct the explicit expression of $U(x,y)$, we expand it around $U(x,x) = \mathbb{1}$. We demand that $U$ is a member of the Lie group, i.e. it can be expanded into a convergent series,

$$U(x+\epsilon\hat{n},x) = \mathbb{1} - i\epsilon n^{\mu} g A_{\mu}(x) + \mathcal{O}(\epsilon^2), \tag{13}$$

with $g$ a constant, which is identified as the *coupling constant*, and $A_\mu$ the gluon field. By inserting the series into eq. (8), we see that $A^\mu$ transforms as

$$A^{\mu} \longrightarrow A^{\mu\prime} = \Omega(x)\left(A^{\mu}(x) + \frac{i}{g}\partial_{\mu}\Omega(x)\right)\Omega(x)^{\dagger}. \tag{14}$$

Using again the series and inserting it now into eq. (10), $D_\mu$ takes the form

$$D^{\mu} = \partial^{\mu} + igA^{\mu}. \tag{15}$$

Comparing to the free Langrangian we get an extra term

$$\mathcal{L}_{\text{int}} = -g\overline{\psi}(x)\gamma_{\mu}A^{\mu}\psi(x), \tag{16}$$

which describes the interaction of quarks and gluons. As gluons carry energy and momentum, we have to add a term to the Lagrangian to describe this feature. Like in electromagnetism we introduce in a similar way the antisymmetric field strength tensor $F^a_{\mu\nu}$ and add the kinetic energy term for gluons

$$\mathcal{L}_g = -\frac{1}{4}F^{\mu\nu}_{a}F_{\mu\nu,a} = -\frac{1}{4}\text{tr}\left[F^{\mu\nu}F_{\mu\nu}\right], \tag{17}$$

where we take the trace over the color indices. The new term is gauge invariant as the field strength tensor transforms like [13]

$$F^{\mu\nu} \longrightarrow \Omega(x)F^{\mu\nu}\Omega(x)^{\dagger}. \tag{18}$$

The non-abelian feature of QCD will be obvious if we look at $F^{\mu\nu}$ which can be written as

$$\begin{aligned} F^{\mu\nu} = -\frac{i}{g}\left[D^{\mu},D^{\nu}\right] &= -\frac{i}{g}\left(\left[\partial^{\mu},\partial^{\nu}\right] + ig\left(\left[\partial\mu,A^{\nu}\right] - \left[\partial^{\nu},A^{\mu}\right]\right) - g^2\left[A^{\mu},A^{\nu}\right]\right) \\ &= \partial^{\mu}A^{\nu}(x) - \partial^{\nu}A^{\mu}(x) + ig\underbrace{\left[A^{\mu}(x),A^{\nu}(x)\right]}_{=A^{\mu}_{a}A^{\nu}_{b}\left[\frac{\lambda^a}{2},\frac{\lambda^b}{2}\right]}. \end{aligned} \tag{19}$$

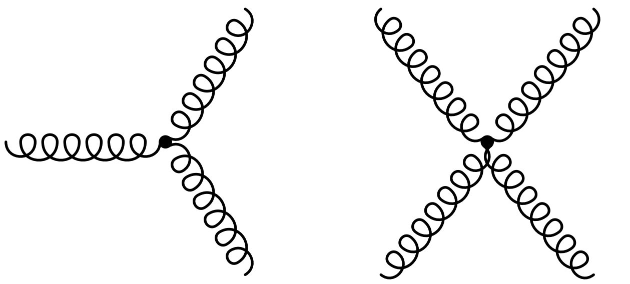

**(a)** Cubic term **(b)** Quartic term

**Figure 1:** Schematic of the self-interaction of gluons. The dots represent the interaction vertices and the curly lines the gluon propagators

With the structure constants $f_{abc}$ we can determine the commutation relation

$$\left[\frac{\lambda^a}{2},\frac{\lambda^b}{2}\right] = i f_{abc}\frac{\lambda^c}{2}. \tag{20}$$

Unlike in QED, the last term on the right-hand side of eq. (19) does not vanish. Inserting the field strength tensor eq. (19) into the gluonic Langrangian eq. (17), we see that cubic and quartic terms in $A_\mu$ appear. These terms give rise to self-interactions of the gluons. In Figure 1 a schematic picture of the self-interaction is shown. To obtain the full Lagrangian density, we add the quark and gluon terms,

$$\mathscr{L}_{\text{QCD}} = \underbrace{\mathscr{L}_{\text{free}} + \mathscr{L}_{\text{g}}}_{=\mathscr{L}_0} + \mathscr{L}_{\text{int}} = \overline{\psi}(x)\left(i\gamma_\mu D^\mu - m\right)\psi(x) - \frac{1}{4}\text{tr}\left[F^{\mu\nu}F_{\mu\nu}\right] \tag{21}$$

## 1.3 Correlation functions and perturbative quantum field theory

In general we are interested in the expectation value of an observable $Q$. We obtain this value by employing the *path integral formulation*

$$\langle Q\rangle = \frac{1}{Z}\int \mathscr{D}\psi\mathscr{D}\overline{\psi}\mathscr{D}A \exp\left(\frac{i}{\hbar}S\left(\psi,\overline{\psi},A\right)\right)Q(\overline{\psi},\psi,A), \tag{22}$$

with $Z$ a normalization factor defined as

$$Z\left[\psi\overline{\psi}\right] = \int \mathscr{D}\psi\mathscr{D}\overline{\psi}\exp\left(\frac{i}{\hbar}S\left(\psi\overline{\psi}\right)\right). \tag{23}$$

$S = \int dx^4 \mathscr{L}_{QCD}$ is the underlying action and $\mathscr{D}\psi = \lim_{N\to\infty}\prod_{n=1}^{N} d\psi_n$, the "sum over all" fields $\psi_n$, analog $\mathscr{D}A$. (From now on we use natural units, $\hbar = c = 1$). Let us be more specific: for simplicity we want to evaluate the amplitude for propagation of a particle between two space-time points 0 and $x$. This quantity can be evaluated by

$$\langle\psi(x)\overline{\psi}(x)\rangle = \frac{1}{Z}\int \mathscr{D}\psi\mathscr{D}\overline{\psi}\mathscr{D}A \exp\left(iS\left(\psi,\overline{\psi},A\right)\right)\psi(x)\overline{\psi}(0) \tag{24}$$

and is called *two-point correlation function* (more on correlation functions can be found in section 1.7.1 ). For most $S$ we cannot evaluate the path integral explicitly. Specifically the interacting term $\mathscr{L}_{\text{int}}$ causes an unsolvable integral. If we assume $g \ll 1$, we can expand $S$,

$$\langle\psi(x)\overline{\psi}(x)\rangle \approx \frac{1}{Z}\int \mathscr{D}\psi\mathscr{D}\overline{\psi}\mathscr{D}A \exp\left(iS_0\left(\psi,\overline{\psi}\right)\right)\left(1+igS_{\text{int}}-\frac{g^2}{2}S_{\text{int}}^2\right)\psi(x)\overline{\psi}(0). \tag{25}$$

These integrals are integrable (see [8]). The expansion is only valid if the coupling is small. We have to consider the striking property of QCD: *asymptotic freedom*.

## 1.4 The running coupling $\alpha_s$

Asymptotic freedom states that the *strong coupling* $\alpha_s = \dfrac{g^2}{4\pi}$ between quarks gets smaller, when the distance $r$ becomes shorter or equally the momentum transfer $Q \sim \dfrac{1}{r}$ gets bigger. Gross, Politzer and Wilczek were rewarded with the Nobel prize in 2004 for the discovery of asymptotic freedom [17]. The dependence of a coupling $\alpha$ in any quantum field theory on the distance or momentum scale $\mu$ can be determined by the following differential equation (renormalization group equation) [7]

$$\mu\frac{d\alpha(\mu)}{d\mu} = \beta(\alpha(\mu)). \tag{26}$$

The beta function $\beta$ is usually computed in perturbation theory, for QCD the function is given by

$$\beta(\alpha) = -\underbrace{\left(11-\frac{2n_f}{3}\right)}_{\beta_0}\frac{\alpha_s^2}{2\pi} \tag{27}$$

with $n_f$ the number of quark flavors. Solving the renormalization group equation we get

$$\alpha_s(\mu) = \frac{2\pi}{\beta_0 \ln\left(\mu/\Lambda\right)}. \tag{28}$$

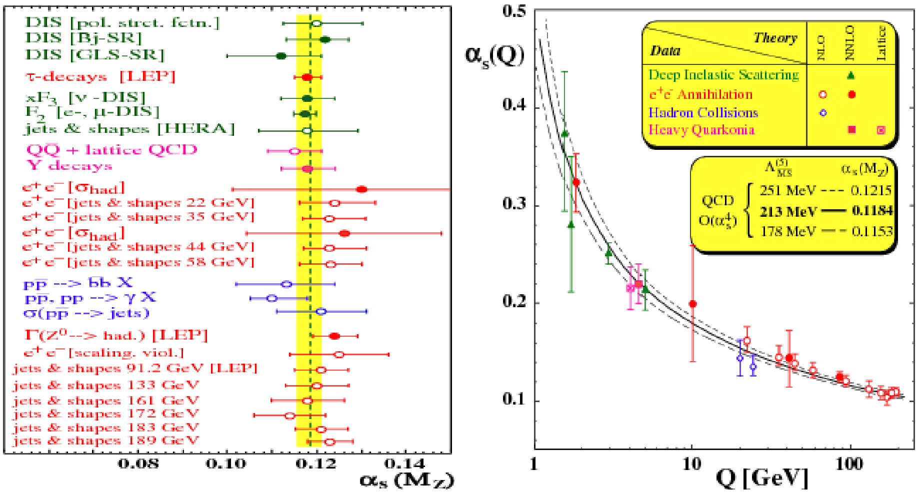


**Figure 2:** Left: Summary of $\alpha_s$ at $M_Z$. Right: $\alpha_s$ in dependence of the momentum transfer Q, taken from [18]

The logarithm in the denominator shows clearly that $\alpha_s(\mu) \longrightarrow 0$ for $\mu \longrightarrow \infty$. The parameter $\Lambda$ is determined to $\Lambda \sim 250\,\mathrm{MeV}$ [7]. Figure 2 shows the coupling determined from different processes in momentrum transfer Q dependence (right) and a summary at the Z-boson mass $M_Z$ (left). So at low-energy a treatment with perturbation theory is not possible . In 1974 Ken Wilson introduced in his paper *"Confinement of Quarks"* [12] a gauge theory on a space-time lattice. In the next section we want see how this makes QCD at low energy possible.

## 1.5 QCD on the Lattice

In Lattice QCD we use Euclidean space-time. The Wick rotation to imaginary times $t \to -it$ leads to Euclidean metric. Next we replace the Euclidean space-time continuum by a discrete 4-dimensional lattice

$$\Lambda = \left\{ x \in \mathbb{R}^4 \middle| \frac{x_1}{a}, \frac{x_2}{a}, \frac{x_3}{a} = 0, \ldots, N_L - 1; \frac{x_0}{a} = 0, 1, \ldots, N_T - 1 \right\}, \tag{29}$$

where $N_L$ and $N_T$ denotes the lattice points in spatial and time direction and $x_\mu = an$, $\mu = \{0, \ldots, 3\}$ the physical space-time point. The gap between two lattice points is $a$, the *lattice spacing*. The lattice has a size of $L = N_L \cdot a$ in spatial and $T = N_T \cdot a$ in time direction. The dual lattice $\tilde{\Lambda}$ can be obtained via a Fourier transform [26]

$$\tilde{\Lambda} = \left\{ p \in \mathbb{R}^4 \middle| p_0 = \frac{2\pi}{T}\left(n_0 - \frac{N_T}{2} + 1\right), \, p_i = \frac{2\pi}{L}\left(n_i - \frac{N_L}{2} + 1\right) \right\}. \tag{30}$$

The dual lattice shows, that the momenta are quantized in units of $2\pi/T$ and $2\pi/L$. As there is a minimal distance, the lattice spacing $a$, we also see a cutoff of momenta in the range [14]

$$-\frac{\pi}{a} < p_\mu \leq \frac{\pi}{a}. \tag{31}$$

For convenience we use the integer value $n$ in the following formulas. We place the fermions at the lattice points only, so we have finite dimensional objects $\psi(n)$ and $\overline{\psi}(n)$, where all indices except the space-time coordinate are suppressed for simplicity.

## 1.6 Discretization of action

The following derivation is inspired from [13], likewise it is recommended for more details. At first we begin with the action of a free fermion $S_{free}$ ( $A_\mu$= 0) in Euclidean space

$$S_{\text{free}} = \int dx^4 \overline{\psi}(x) \left(\gamma_\mu \partial^\mu + m_0\right) \psi(x). \tag{32}$$

By discretizing the action we replace the space-time variable $x$ by a discrete variable $n$. The integral as well as the partial derivative are affected. The integral has to be replaced with a sum over $\Lambda$, whereas for the derivative we use a finite difference

$$\partial_\mu \psi(x) \longrightarrow \frac{1}{2a} \left(\psi(n+\hat{\mu}) - \psi(n-\hat{\mu})\right), \tag{33}$$

with $n \pm \hat{\mu}$ the neighboring point of $n$ in $\pm$ $\mu$-direction. Then the action reads

$$S_{\text{free}} = a^4 \sum_{n\in\Lambda} \overline{\psi}(n) \left( \sum_{\mu=1}^{4} \frac{1}{2a} \left(\psi(n+\hat{\mu}) - \psi(n-\hat{\mu})\right) + m_0 \psi(n) \right). \tag{34}$$

Like in the continuum case , the QCD action is invariant under local SU(3) rotations. We employed the infinitesimal gauge transporter $U(y,x)$ to restore the invariance. However, to transport the gauge transformation on a finite path $\gamma$ from x to y, we have to use infinitesimal segments

$$U_\gamma(y,x) = U(y,x_n) U(x_n, x_{n-1}) \ldots U(x_1, x). \tag{35}$$

It can be shown, that $U_\gamma$ can be written as [8]

$$U_\gamma(y,x) = \mathscr{P} \exp\left(-i \int_\gamma A_\mu(x) dx^\mu\right), \tag{36}$$

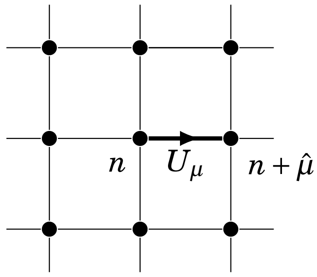


**Figure 3:** The link variable $U_\mu(n)$ connects the sites $n$ and $n+\hat{\mu}$

where $\mathscr{P}$ denotes the path-ordering. Since there is no infinitesimal spacing on the lattice we write [13]

$$\begin{aligned} U_\mu(n) &= \exp\left(\mathrm{iaA}_\mu(\mathrm{n})\right), \\ U_{-\mu}(n) &= U_\mu(n-\hat{\mu})^\dagger = \exp\left(-\mathrm{iaA}_\mu(\mathrm{n}-\hat{\mu})\right). \end{aligned} \tag{37}$$

$U_\mu(n)$, which is depicted in Figure 3, is referred to as a *link variable*, as it exist on the link between the sites $n$ and $n+\hat{\mu}$. With $U_\mu(n)$ we can generalize the free fermion action eq. (34) to

$$S_N = a^4 \sum_{n\in\Lambda} \overline{\psi}(n)\left(\sum_{\mu=1}^{4} \frac{\gamma_\mu}{2a}\left(U_\mu(n)\psi(n+\hat{\mu}) - U_{-\mu}(n)\psi(n-\hat{\mu})\right) + m_0\psi(n)\right). \tag{38}$$

It shows discretization effects of order $\mathscr{O}(a^2)$, and we recover the continuum form. We write eq. (38) as

$$S_N = a^4 \sum_{n,m\in\Lambda} \overline{\psi}(n)D(n,m)\psi(m),$$

with the *Dirac Operator*

$$D(n,m) = \sum_{\mu=1}^{4} \frac{\gamma_\mu}{2a}\left(U_\mu(n)\delta_{n+\hat{\mu},m} - U_{-\mu}(n)\delta_{n-\hat{\mu},m}\right) + m_0\delta_{n,m}. \tag{39}$$

To construct the full action we need to add the gluonic or gauge field part. We build the shortest, nontrivial closed loop on the lattice, which is referred to as *plaquette*. The smallest loop is depicted in Figure 4 and can be defined as

$$\begin{aligned} P_{\mu,\nu} &= U_\mu(n)U_\nu(n+\hat{\mu})U_{-\mu}(n+\hat{\mu}+\hat{\nu})U_{-\nu}(n+\hat{\nu}) \\ &= U_\mu(n)U_\nu(n+\hat{\mu})U_\mu(n+\hat{\nu})^\dagger U_\nu(n)^\dagger, \end{aligned} \tag{40}$$

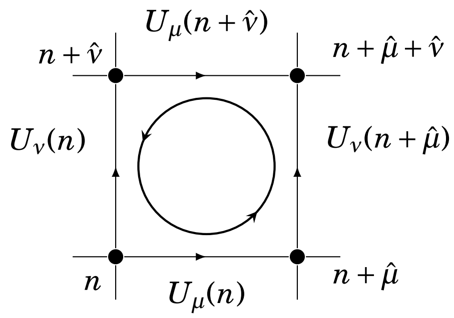


**Figure 4:** $P_{\mu,\nu}$ as the smallest loop. It is build up by the gauge field U(n)

where we used $U_{-\lambda}(n) = U_\lambda(n-\hat{\lambda})^\dagger$. To construct a gauge-invariant object, we take the trace over a closed loop of link variables (plaquette). The *Wilson plaquette action* is defined by

$$S_G = \frac{2}{g^2} \sum_{n\in\Lambda} \sum_{\mu<\nu} \mathrm{Re}\,\mathrm{tr}\left[\mathbb{1} - P_{\mu,\nu}(n)\right]. \tag{41}$$

Taking the limit a $\longrightarrow$ 0, the Wilson plaquette action also approaches the continuum limit,

$$\frac{2}{g^2} \sum_{n\in\Lambda} \sum_{\mu<\nu} \mathrm{Re}\,\mathrm{tr}\left[\mathbb{1} - U_{\mu\nu}(n)\right] = \frac{a^4}{2g^2} \sum_{n\in\Lambda} \sum_{\mu<\nu} \mathrm{tr}\left[F_{\mu\nu}(n)^2\right] + \mathcal{O}(a^2). \tag{42}$$

### 1.6.1 Fermion doubling and Wilson fermions

Looking at the Fourier transforms of the lattice Dirac operator we face another problem. For simplicity we are looking at a trivial gauge field, i.e. $U_\mu = \mathbb{1}$. Taking the Fourier transform of eq. (39) for the trivial case we get

$$\begin{aligned} \mathscr{F}(D(n,m)) &= \frac{1}{|\Lambda|} \sum_{n,m\in\Lambda} e^{-ipna} D(n,m) e^{iqma} \\ &= \frac{1}{|\Lambda|} \sum_{n\in\Lambda} e^{-i(p-q)na} \left( \sum_{\mu=1}^{4} \frac{\gamma_\mu}{2a} \left( e^{iq_\mu a} - e^{-iq_\mu a} \right) + m_0 \mathbb{1} \right) \\ &= \delta(p-q) \underbrace{\left( m_0 \mathbb{1} + \frac{i}{a} \sum_{\mu=1}^{4} \gamma_\mu \sin(p_\mu a) \right)}_{\tilde{D}(p)}. \end{aligned} \tag{43}$$

We applied two independent Fourier transform, one to $n$ and the other to $m$. In the second step we applied it to $m$ and used $q \cdot \hat{\mu} = q_\mu$. In order to calculate the inverse $\tilde{D}^{-1}(p)$ in momentum space we use following formula

$$\left(a\mathbb{1} + i\sum_{\mu}\gamma_\mu b_\mu\right)^{-1} = \frac{a\mathbb{1} - i\sum_\mu \gamma_\mu b_\mu}{a^2 + \sum_\mu b_\mu^2} \tag{44}$$

and get

$$\tilde{D}(p)^{-1} = \frac{m\mathbb{1} - ia^{-1}\sum_\mu \gamma_\mu \sin(p_\mu a)}{m^2 + a^{-2}\sum_\mu \sin(p_\mu a)^2}. \tag{45}$$

Taking the limit $a \longrightarrow 0$ and setting the mass $m = 0$ we get

$$\tilde{D}(p)^{-1} \overset{a\longrightarrow 0}{\longrightarrow} \frac{-i\sum_\mu \gamma_\mu p_\mu}{p^2}. \tag{46}$$

This inverse is referred to as *quark propagator* in momentum space. Comparing eq. (45) and eq. (46) we see that the continuum version has one pole at $p = (0,0,0,0)$, whereas the lattice version has additional poles. As mentioned for the dual lattice, the momentum space is $p_\mu \in \left(-\frac{\pi}{a}, \frac{\pi}{a}\right]$. Looking at eq. (45) we see the following poles due to the sine in the denominator

$$p = \left(\tfrac{\pi}{a}, 0, 0, 0\right), \left(0, \tfrac{\pi}{a}, 0,\ 0\right), ..., \left(\tfrac{\pi}{a}, \tfrac{\pi}{a}, \tfrac{\pi}{a}, \tfrac{\pi}{a}\right). \tag{47}$$

With the binomial coefficient $\binom{n}{k} = \frac{n!}{k!(n-k)!}$, we get the number of additional poles

$$\binom{4}{1} + \binom{4}{2} + \binom{4}{3} + \binom{4}{4} = 15. \tag{48}$$

These additional unwanted, because unphysical poles are called *doublers*. To get rid of the doublers, Wilson suggested to add an extra term to the momentum space Dirac operator that vanishes in the continuum limit,

$$\tilde{D}(p) = m_0\mathbb{1} + \frac{i}{a}\sum_{\mu=1}^{4}\gamma_\mu \sin(p_\mu a) + \underbrace{\mathbb{1}\frac{1}{a}\sum_{\mu=1}^{4}\left(1 - \cos(p_\mu a)\right)}_{\textit{Wilson term}} \tag{49}$$

The extra term, the *Wilson term* eliminates the unwanted poles. In position space the Wilson term can be written as

$$-a\sum_{\mu=1}^{4}\frac{1}{2a^2}\left(U_\mu(n)\delta_{n+\hat{\mu},m} - 2\delta_{n,m} + U_{-\mu}(n)\delta_{n-\hat{\mu},m}\right), \tag{50}$$

and inserting it in eq. (39) we obtain

$$D_W(n,m) = \frac{1}{2a}\sum_{\mu=1}^{4}\left(\gamma_\mu - \mathbb{1}\right)U_\mu(n)\delta_{n+\hat{\mu},m+} - \frac{1}{2a}\sum_{\mu=1}^{4}\left(\gamma_\mu + \mathbb{1}\right)U_{-\mu}(n)\delta_{n-\hat{\mu},m+} + \left(m_0 + \frac{4}{a}\right)\delta_{n,m}, \tag{51}$$

the *Wilson Dirac operator*. In contrast to the naive fermion action, the Wilson action shows discretization effects of order $\mathcal{O}(a)$. They can be removed by adding an improvement term (see below). We can separate $D_W$ into a part proportional to the unit matrix $\mathbb{1}$ and a part proportional to a matrix $H$ which connects neighboring lattice points,

$$D_W = \frac{1}{2a\kappa}\mathbb{1} - \frac{1}{2}H. \tag{52}$$

$H$ is called the *hopping matrix*, and $\kappa$ is the hopping parameter defined as

$$\kappa = \frac{1}{2\left(am_0 + 4\right)}. \tag{53}$$

Combining the fermionic $S_F$ and gluonic part $S_G$ we get the full *Wilson action*

$$S_W = \underbrace{a^4 \sum_{n,m\in\Lambda} \overline{\psi}(n) D_W(n,m)\psi(m)}_{S_F} + \underbrace{\frac{\beta}{3}\sum_{n\in\Lambda}\sum_{\mu<\nu} \mathrm{Re}\ \mathrm{tr}\left[\mathbb{1} - P_{\mu,\nu}(n)\right]}_{S_G}, \tag{54}$$

where the coupling constant $g$ was rewritten as the numerical parameter

$$\beta = \frac{6}{g^2}. \tag{55}$$

Adding the Wilson term causes the breaking of chiral symmetry, i.e.

$$\gamma_5 D_W + D_W \gamma_5 \neq 0. \tag{56}$$

With the Wilson term an additive renormalisation is generated

$$m = \frac{1}{2a}\left(\frac{1}{\kappa} - \frac{1}{\kappa_c}\right) = m_0 - m_c, \tag{57}$$

with the critical hopping parameter $\kappa_c$.

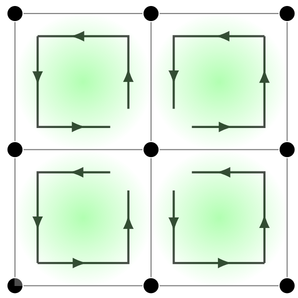

**Figure 5:** $G_{\mu\nu}$ as the sum of $U_{\mu\nu}(n)$. It is reminiscent of a clover leaf.

### 1.6.2 $\mathcal{O}$(a)-improvement

As mentioned before, the lattice action leads to discretization effects of $\mathcal{O}(a)$ for Wilson fermions and $\mathcal{O}(a^2)$ for gauge fields. The idea of removing the leading discretization effects by adding an extra terms and matching its coefficient appropriately is called the Symanzik improvement program [19]. Sheikholeslami and Wohlert [20] reduced the discretization effects in the fermionic part from $\mathcal{O}(a)$ to $\mathcal{O}(a^2)$ with the following expression

$$S_I = S_W + c_{SW} a^5 \sum_{n\in\Lambda} \sum_{\mu<\nu} \overline{\psi}(n) \frac{1}{2} \sigma_{\mu\nu} \hat{F}_{\mu\nu}(n) \psi(n), \tag{58}$$

where $\sigma_{\mu\nu} = [\gamma_\mu, \gamma_\nu]/2i$. $c_{SW}$ is referred to as the *Sheikholeslami-Wohlert coefficient*. The field strength tensor is

$$\hat{F}_{\mu\nu}(n) = \frac{-i}{8a^2} \left( G_{\mu\nu}(n) - G_{\nu\mu}(n) \right), \tag{59}$$

where $G_{\mu\nu}$ is the sum of four plaquettes $P_{\mu,\nu}$

$$G_{\mu\nu}(n) = P_{\mu,\nu} + P_{\nu,-\mu} + P_{-\mu,-\nu} + P_{-\nu,\mu}. \tag{60}$$

$G_{\mu\nu}(n)$ takes the shape of a clover leaf (see Figure 5), it is often called *clover term*. We will use the $\mathcal{O}(a)$-improved Wilson action for the calculation of matrix elements. Now that the action is fully discretized we continue with evaluating the path integral (22) and use the Wick theorem to calculate the path integral.

## 1.7 Requirements for computable path integrals

To calculate the expectation value of an observable $\langle Q \rangle$ we have to evaluate the integral

$$\langle Q \rangle = \frac{1}{Z} \int \mathcal{D}\left[\psi, \overline{\psi}, U\right] Q \left[\psi, \overline{\psi}, U\right] e^{-S_E}, \tag{61}$$

where Z denotes the partition function

$$Z = \int \mathscr{D}\left[\psi,\overline{\psi},U\right] e^{-S_E}, \tag{62}$$

and $S_E$ is the Euclidean action. It is convenient to separate the action into a fermionic and a gauge field part,

$$\langle Q\rangle = \langle\langle Q\rangle_F\rangle_G = \frac{1}{Z}\int \mathscr{D}[U]\, e^{-S_G[U]}\int \mathscr{D}\left[\psi,\overline{\psi}\right] e^{-S_F[\psi,\overline{\psi},U]} Q\left[\psi,\overline{\psi},U\right]. \tag{63}$$

### 1.7.1 Fermionic expectation value

Here we derive the calculation for the vacuum expectation value of a product of n fermion fields, also known as an *n-point correlation function*. They can be interpreted as the propagation of particles between two spacetime points $n$ and $m$. In this thesis we will use two- and three-point functions, which provide our desired measurable quantities, the mass and axial charge (see section 2.5 and 2.8). The n-point function can be written as

$$\langle Q\rangle_F = \langle 0|\,\hat{\psi}(n_1)\hat{\overline{\psi}}(m_1)\,...\,\hat{\psi}(n_n)\hat{\overline{\psi}}(m_n)\,|0\rangle = \langle \psi(n_1)\overline{\psi}(m_1)\,...\,\psi(n_n)\overline{\psi}(m_n)\rangle, \tag{64}$$

and we know how to calculate the expectation value using the action:

$$\begin{aligned}\langle Q\rangle_F &= \frac{1}{Z_F[U]}\int \mathscr{D}[\psi,\overline{\psi}] e^{-S_F[\psi,\overline{\psi},U]} Q\left[\psi,\overline{\psi},U\right],\\ Z_F[U] &= \int \mathscr{D}\left[\psi,\overline{\psi}\right] e^{-S_F[\psi,\overline{\psi},U]}.\end{aligned} \tag{65}$$

For clarity we use the index notation, setting

$$\psi(n) = \eta_i, \quad D(n,m) = D_{ik} \quad \psi(m) = \eta_k \qquad \text{with} \quad i,k = 1...N. \tag{66}$$

Looking at $S_F$ in eq. (54)

$$Z_F = \int \prod_{j=1}^{N} d\eta_j d\overline{\eta}_j \exp\left(-\sum_{i,k=1}^{N} \overline{\eta}_i D_{ik}\eta_k\right). \tag{67}$$

Now we apply a transformation such that

$$\eta'_i = -\sum_{k=1}^{N} D_{ik}\eta_k. \tag{68}$$

As we are dealing with fermions, i.e. with anti-commuting variables, we treat $\eta$ as *Grassmann numbers*, with [13]

$$\eta_i\eta_j = -\eta_j\eta_i \Rightarrow \eta_i^2 = 0. \tag{69}$$

One can show [13] that the transformation of the measure can be written as

$$\prod_{j=1}^{N} d\eta_j d\overline{\eta}_j = \det[D] \prod_{j=1}^{N} d\eta'_j d\overline{\eta}_j. \tag{70}$$

Now we get

$$Z_F = \det[D] \int \prod_{j=1}^{N} d\eta'_j d\overline{\eta}_j \exp\left(\sum_{i=1}^{N} \overline{\eta}_i \eta'_i\right) = \det[D] \prod_{j=1}^{N} \int d\eta'_j d\overline{\eta}_j \exp\left(\overline{\eta}_j \eta'_j\right). \tag{71}$$

Notice that we shifted the product symbol in front of the integral. If we expand the exponential function in a power series and consider the nilpotency of Grassmann numbers ($\mathcal{O}(\eta^2) = 0$) we obtain

$$Z_F = \det[D] \prod_{j=1}^{N} \int d\eta'_j d\overline{\eta}_j \left(1 + \overline{\eta}_j \eta'_j\right) = \det[D], \tag{72}$$

where we used that $\int d\eta_j 1 = 0$ and $\int d\eta_j \eta_j = 1$ [13]. The solution is known as *fermion determinant* and the integral as *Matthews-Salam formula*. The determinant describes the *sea quarks*, it can be written as a sum over closed loops of gauge field link variables [13]. Setting $\det[D] = 1$ is known as the *quenched approximation*. It was a common practice in the 1980s and 1990s and neglects the quark contribution from the fermion vacuum. Today the simulations are done with dynamical quark flavors. Going back to eq. (65) we have still to evaluate the part $\langle Q \rangle_F^{un}$ (the fermionic expectation value without the partition function)

$$\langle Q \rangle_F^{un} = \int \mathcal{D}[\psi, \overline{\psi}] e^{-S_F[\psi,\overline{\psi},U]} Q\left[\psi, \overline{\psi}, U\right]. \tag{73}$$

Again we use the index notation and $Q = \eta_{i_1}\overline{\eta}_{j_1} \ldots \eta_{i_n}\overline{\eta}_{j_n}$, so that

$$\langle Q \rangle_F^{un} = \int \prod_{j=1}^{N} d\eta_j d\overline{\eta}_j \exp\left(\sum_{i,k=1}^{N} \overline{\eta}_i D_{ik} \eta_k\right) \eta_{i_1}\overline{\eta}_{j_1} \ldots \eta_{i_n}\overline{\eta}_{j_n}. \tag{74}$$

$\langle Q \rangle_F^{un}$ can be calculated by considering the *generating functional for fermions*

$$W\left[\theta,\overline{\theta}\right] = \int \prod_{j=1}^{N} d\eta_j d\overline{\eta}_j \exp\left( \sum_{i,k=1}^{N} \overline{\eta}_i D_{ik} \eta_k + \sum_{i=1}^{N} \overline{\theta}_i \eta_i + \sum_{i=1}^{N} \overline{\eta}_i \theta_i \right), \tag{75}$$

where $\theta_i$ and $\overline{\theta}_i$ can bee seen as source terms. The connection of $W\left[\theta,\overline{\theta}\right]$ and the fermionic expectation value is ( $Q = \eta_{i_1}\overline{\eta}_{j_1} \ldots \eta_{i_n}\overline{\eta}_{j_n}$)

$$\langle \eta_{i_1}\overline{\eta}_{j_1} \ldots \eta_{i_n}\overline{\eta}_{j_n} \rangle_F = \frac{1}{Z_F} \frac{\partial}{\partial \theta_{j_1}} \frac{\partial}{\partial \overline{\theta}_{i_1}} \ldots \frac{\partial}{\partial \theta_{j_n}} \frac{\partial}{\partial \overline{\theta}_{i_n}} W\left[\theta,\overline{\theta}\right] \bigg|_{\theta,\overline{\theta}=0}. \tag{76}$$

To evaluate $W[\theta,\overline{\theta}]$ we rewrite the exponent such that

$$\overline{\eta}_i D_{ik} \eta_k + \overline{\theta}_i \eta_i + \overline{\eta}_i \theta_i = \left(\overline{\eta}_i + \overline{\theta}_j \left(D^{-1}\right)_{ji}\right) D_{ik} \left(\eta_k + \left(D^{-1}_{kl}\right)\theta_l\right) - \overline{\theta}_n \left(D^{-1}\right)_{nm} \theta_m. \tag{77}$$

Employing the transformation

$$\eta'_k = \eta_k + \left(D^{-1}\right)_{kl} \theta_l, \quad \overline{\eta}'_i = \overline{\eta}_i + \overline{\theta}_j \left(D^{-1}\right)_{ji} \tag{78}$$

and using the Matthews-Salam formula we get [13]

$$W\left[\theta,\overline{\theta}\right] = \det[D] \, \exp\left( - \sum_{n,m}^{N} \overline{\theta}_n \left(D^{-1}\right)_{nm} \theta_m \right). \tag{79}$$

The fermionic expectation is then (see eq. 76)

$$\langle \eta_{i_1}\overline{\eta}_{j_1} \ldots \eta_{i_n}\overline{\eta}_{j_n} \rangle_F = (-1)^n \sum_{\mathscr{P}(1,2,\ldots,n)} \mathrm{sign}(\mathscr{P}) (D^{-1})_{i_1 j_{\mathscr{P}_1}} \ldots (D^{-1})_{i_n j_{\mathscr{P}_n}}. \tag{80}$$

So the expectation value is the sum over all permutations $\mathscr{P}$ of products of the inverse Dirac operator of pair-wise quark contractions. It vanishes for different numbers of $\eta_i$ and $\overline{\eta}_j$. This is known as *Wicks's theorem*.

### 1.7.2 Gluonic expectation value

To get the full expectation value we have to sum also over all gauge field configuration $U$. The gauge field part of the expectation value is

$$\langle Q \rangle_G = \frac{1}{Z} \int \mathscr{D}[U] e^{-S_G[U]} Z_F[U] Q[U] \tag{81}$$

Considering the $n_f$ mass parameters of the sea quarks $m_i$ we get [29]

$$\langle Q\rangle_G = \frac{1}{Z}\int \mathscr{D}[U]\, e^{-S_G[U]} Q[U] \prod_{i=1}^{n_f} \det[D+m_i] = \int \mathscr{D}[U] P(U) Q[U], \tag{82}$$

with the statistical weight

$$P(U) = \frac{1}{Z}\prod_{i=1}^{n_f} \det[D+m_i]\, e^{-S_G[U]}. \tag{83}$$

The normalization Z is fixed by imposing

$$\langle \mathbb{1}\rangle = \frac{1}{Z}\int D[U] e^{-S_G[U]} \prod_{i=1}^{n_f} \det[D+m_i] \equiv 1. \tag{84}$$

To evaluate the integral, one has to integrate over all lattice sites and all free variables. Avoiding the high-dimensional integral, the integration of eq. (81) is usually evaluated by employing Monte Carlo integration. The generation of gauge field configuration are done in a *Markov chain*. The gauge fields are correlated with fields generated at prior Monte carlo steps. Starting from an arbitrary configuration $U_n$, the Markov chain generates subsequent configurations $U_n$

$$U_0 \longrightarrow U_1 \longrightarrow U_2 \longrightarrow \ldots.$$

The expectation value can be estimated by the ensemble mean,

$$\langle Q\rangle_G = \frac{1}{N}\sum_i^N Q[U_i] + \mathcal{O}\left(\frac{1}{\sqrt{N}}\right), \tag{85}$$

where $\mathcal{O}\left(\frac{1}{\sqrt{N}}\right)$ is the estimated error of the gauge average and $U_i,\ i = 1,\ldots N$ the ensemble of the gauge field configurations generated by the Markov chain.

## 1.8 Scale setting

In Lattice QCD all observables are dimensionless. To convert them into physical units we need to determine the lattice spacing $a$, which is not known a priori. There are several techniques to determine the lattice spacing $a$, of which one is setting it with a physical hadron mass. The simulated mass using lattice QCD is a dimensionless number $am_{\mathrm{lat}}$. By relating this number to an experimentally

| id | $\beta$ | $N_L$ | $N_T$ | $\kappa_u$ | $\kappa_s$ | $m_K$[MeV] | $m_\pi$[MeV] | $m_\pi$ L |
|---|---|---|---|---|---|---|---|---|
| H102 | 3.4 | 32 | 96 | 0.136865 | 0.136549339 | 350 | 440 | 4.9 |
| H105 | 3.4 | 32 | 96 | 0.136970 | 0.13634079 | 280 | 460 | 3.9 |
| C101 | 3.4 | 48 | 96 | 0.137030 | 0.136222041 | 220 | 470 | 4.7 |

**Table 2:** Configurations used in this thesis. The values are taken from [62].

determined mass $m_{\text{phys}}$

$$a[\text{fm}] = \frac{am_{\text{lat}}}{m_{\text{phys}}[\text{MeV}]}\hbar c[\text{MeV fm}] \tag{86}$$

with $\hbar c$=197.327 MeV we get the lattice spacing. A typical choice of $m_{\text{lat}}$ is the mass of the $\Omega$-baryon [25]. It is stable in QCD and its mass is only weakly dependent on the light quark mass.

## 1.9 Lattice set-up

The gauge ensembles, used in this thesis are shown in table 2 . The size of the lattices are $N_T \times N_L^3$ . They were generated with $N_f$=2+1 dynamical quark flavors by the Coordinated Lattice Simulation (CLS) effort. There are 2 symmetric flavors fermions, up and down, and one fermion different from the other two, the strange quark. The ensembles were generated with O(a) improved Wilson fermion [21]. We use a lattice spacing of $a$=0.086 fm [62]. As the four-dimensional lattice is bounded by $N_L$ in the spatial direction and by $N_T$ in the time direction, we have to implement boundary conditions to simulate an infinite space. The spatial direction is taken to be a three-dimensional torus [22], i.e. they satisfy periodic boundary conditions,

$$\psi(n + N_L\hat{n}_k) = \psi(n), \qquad U_\mu(n + N_T\hat{n}_k) = U_\mu(n), \tag{87}$$

with $\hat{n}_k$ the spatial direction. For the time direction we use *open boundary* conditions [23]

$$U_\mu(0) = U_\mu(N_T - 1) = 0, \qquad \psi(0) = \psi(N_T - 1) = 0 \tag{88}$$

The simulations are performed using the openQCD package[1] [24]. Notice that the ensembles provide unphysical pion and kaon masses. A chiral extrapolation to the physical mass and to the continuum limit has to be done in order to get the physical observables. In this thesis we extrapolate to the physical mass (see section 5).

[1]Calculations are done on a large amount of lattice sites. This requires high-performance parallel computers. OpenQCD offers a high degree of flexibility when performing the algorithm across multiple processors.

# 2 Numerical Calculation and the axial charge

In this chapter we want to discuss how the calculations of the propagators are done. We introduce the idea of smearing and show contractions for two-point functions. This will be done on the basis of a meson contraction and at the end we extracte the so-called effective mass from the two-point correlator of the $\Lambda$ baryon.

## 2.1 Propagator

The previous chapter shows that the calculation of the expectation value of n-point functions require the inverse Dirac operator, which is the *propagator* (two-point function). The propagator $S(n,l)$ can be obtained from the Dirac equation applied with a source term $J(n,l)$. Setting $J(n,l)$=$\delta_{nl}$ the propagator is just the Green's function

$$\sum_m D(n,m)S(m,l) = \delta_{nl}. \tag{89}$$

Including spin and color indices this equation reads

$$\sum_{m,\beta,b} D(n,m)^{a,b}_{\alpha,\beta} S(m,l)^{b,c}_{\beta,\gamma} = \delta_{nl}\delta_{\alpha\gamma}\delta_{ac}. \tag{90}$$

$S(m,l)^{b,c}_{\beta,\gamma}$ connects a source point with the space-time coordinate $l$, the Dirac indices $\gamma$ and the color indices $c$ ($l$,$\gamma$,$c$) with a sink point ($m$,$\beta$,$b$). The Dirac operator is a matrix of dimension $3\times 4\times N$, due to the 3 colors, 4 Dirac indices, and $N = N_L^3 \times N_T$ lattice points. To extract the propagator on a lattice of e.g. size $3\times 3$ we have to do 12×12×9×9= 11644 calculations. 12×12 refers to the contraction of *all* possible Dirac/color states to *all* possible Dirac/color states and 9×9 to the contraction of *all* lattice points to *all* lattice points. We call such propagator an *all-to-all propagator*. A pictorial representation for 3 matrix entries ( only 3, because of better readability ) is given in figure 6. For our calculation it is sufficient to fix the spacetime-, Dirac- and color indices $(l_0,\gamma_0,c_0)$. Instead of solving eq. (90) we use

$$\sum_{m,\beta,b} D(n,m)^{a,b}_{\alpha,\beta} S(m,l_0)^{b,c_0}_{\beta,\gamma_0} = \delta_{nl_0}\delta_{\alpha\gamma_0}\delta_{ac_0}. \tag{91}$$

This propagator is called a *point-to-all propagator* (see figure 7).

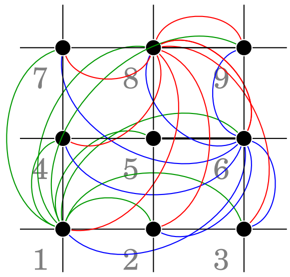


**Figure 6:** *All-to-all propagator*: The propagators are only drawn for the three lattice points 1, 6 and 8.

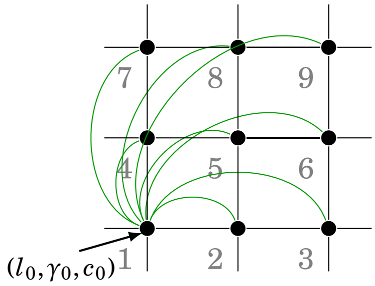


**Figure 7:** Point-to-all propagator. The source point is fixed at $(l_0, \gamma_0, c_0)$

## 2.2 Smearing

With point sources, the signal is highly contaminated with excited states. In order to reduce the influence of these excited states and to get a better signal on the ground state we use a *smeared source*, i.e. we smear th quark fields at the source. This leads to an improvement in small Euclidean time, which provides us with a longer mass plateau. Smearing of the quark fields at the source can be done by

$$\sum_{m,\beta,b} D(n,m)^{ab}_{\alpha,\beta} \tilde{S}(m,l_0)^{b,c_0}_{\beta,\gamma_0} = M(n,k)^{ad}_{\alpha\delta} \delta_{kl_0} \delta_{\delta\gamma_0} \delta_{dc_0}, \tag{92}$$

with the smearing operator $M(n,k)^{ad}_{\alpha\delta}$ and $\tilde{S}(m,l_0)^{b,c_0}_{\beta,\gamma_0}$ the source-smeared propagator. Applying the smearing operator to the source-smeared propagator

$$\hat{\tilde{S}}(n,k)^{ad}_{\alpha\delta} = M(n,m)^{ab}_{\alpha\beta} \tilde{S}(m,k)^{bd}_{\beta\delta}, \tag{93}$$

we get the smeared-smeared propagator which is also smeared at the sink. $M$ has to be chosen such that the excited states are suppressed. For the so-called Wuppertal smearing, we use the ansatz (all indices are suppressed) [27].

$$M = (1 + \alpha H),$$

with H the hopping Matrix (see eq. (52)) and $\alpha$ a tunable parameter. Now one defines an iterative scheme by

$$M = (1 + \alpha H)^k ,$$

with the number $k$ of iterations. Investigating the quark fields, one finds that these are approximately in a Gaussian shape [27]. One can tune $\alpha$ to suppress the contamination from excited states.

## 2.3 Correlator

The two-point function of an arbitrary hadron with the creation operator $O^\dagger(n)$ and the annihilation operator $O(m)$ is

$$C_{2pt} = \left\langle O(n) O^\dagger(m) \right\rangle . \tag{94}$$

The hadron is created at the space-time coordinate $n$ and annihilate at $m$. $O$ is called the *interpolator*, it is made of the quark content of the hadron. For meson we use e.g.,

$$O(n) = \overline{q}_1(n)^a_\alpha \Gamma_{\alpha\beta} q_2(n)^a_\beta , \qquad O^\dagger(m) = \overline{q}_2(m)^b_\gamma \Gamma_{\gamma\delta} q_1(m)^b_\delta , \tag{95}$$

where $q$ represents a quark and $\overline{q}$ an anti-quark with flavor 1 and 2. Note that the color indices of the anti-quark indicates anti-colors. $\Gamma$ denotes one of the 16 independent $\gamma$-matrices. We choose the matrices appropriate to the symmetries of the particle. In table 3 all matrices all listed with the state of the particle. For calculating the meson correlator $\langle O(m) O^\dagger(n) \rangle$ we need to use Wick's Theorem (WT) for

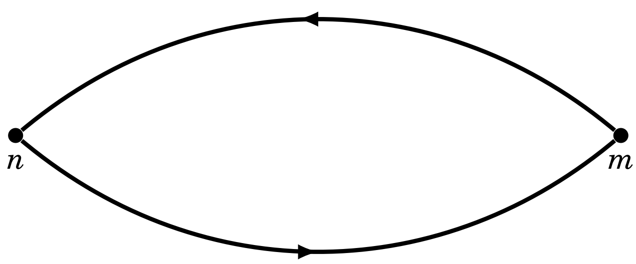


**Figure 8:** Schematic of the two-point function of a meson correlator

| State | $J^{PC}$ | $\Gamma$ | Particles |
|---|---|---|---|
| Scalar | $0^{++}$ | $\mathbb{1}, \gamma_0$ | $f_0, a_0, K_0^*, \ldots$ |
| Pseudoscalar | $0^{-+}$ | $\gamma_5, \gamma_0\gamma_5$ | $\pi^\pm, \pi^0, \eta, K^\pm, K^0, \ldots$ |
| Vector | $1^{--}$ | $\gamma_i, \gamma_0\gamma_i$ | $\rho^\pm, \rho^0, \omega, K^*, \phi, \ldots$ |
| Axial vector | $1^{++}$ | $\gamma_i\gamma_5$ | $a_1, f_1, \ldots$ |
| Tensor | $1^{+-}$ | $\gamma_i\gamma_j$ | $h_1, b_1, \ldots$ |

**Table 3:** Gamma matrices according to the quantum numbers of some particles [13].

the fermionic expectation value,

$$\begin{aligned}
\left\langle O(m)O^\dagger(n)\right\rangle &= \left\langle\left\langle O(m)O^\dagger(n)\right\rangle_F\right\rangle_G \\
&= \left\langle\left\langle \overline{q}_1(n)^a_\alpha \Gamma_{\alpha\beta} q_2(n)^a_\beta \overline{q}_2(m)^b_\gamma \Gamma_{\gamma\delta} q_1(m)^b_\delta \right\rangle_F\right\rangle_G \\
&= -\left\langle \Gamma_{\alpha\beta}\Gamma_{\gamma\delta} \langle q_2(n)^a_\beta \overline{q}_2(m)^b_\gamma\rangle_F \left\langle q_1(m)^b_\delta \overline{q}_1(n)^a_\alpha\right\rangle_F\right\rangle_G \\
&\overset{WT}{=} -\left\langle \Gamma_{\alpha\beta}\Gamma_{\gamma\delta} S_2(n,m)^{ab}_{\beta\gamma} S_1(m,n)^{ba}_{\delta\alpha}\right\rangle_G \\
&= -\langle \mathrm{Tr}[\Gamma S_1(n,m)\Gamma S_2(m,n)]\rangle_G .
\end{aligned}$$

The minus sign appears due to the antisymmetry property of Grassmann variables and the odd number of swaps. In the last line the trace was taken in color and Dirac space. The propagator $S_1(n,m)$ propagate a quark with flavor 1 from space-time $m$ to the point $n$, while $S_2(m,n)$ acts on a quark with flavour 2 in the opposite direction (figure 9). There are also propagators, which propagate from one space-time point back to the same point[1]. This happens when flavor 1 = flavor 2. These propagator are called *quark-disconnected*, while we call the previously discussed ones *quark-connected*. The disconnected part plays e.g. a role for isoscalar quantities. The disconnected part will be omitted, as is it beyond the scope of this thesis. In order to define an interpolator with a given momentum we have to apply a Fourier transformation,

$$\tilde{O}(\boldsymbol{p}, n_t) = \sum_{\boldsymbol{n}=0}^{N} O(\boldsymbol{n}, n_t) e^{-ia\boldsymbol{n}\boldsymbol{p}}, \qquad \tilde{O}^\dagger(\boldsymbol{p}, m_t) = \sum_{\boldsymbol{m}=0}^{N} O(\boldsymbol{m}, m_t) e^{ia\boldsymbol{m}\boldsymbol{p}}. \tag{96}$$

For a general hadron correlator the transformation yields

$$\langle \tilde{O}(\boldsymbol{p}, n_t)\tilde{O}^\dagger(\boldsymbol{p}, m_t)\rangle = \sum_{\boldsymbol{n},\boldsymbol{m}} e^{-ia\boldsymbol{p}(\boldsymbol{n}-\boldsymbol{m})} \langle O(\boldsymbol{n}, n_t) O^\dagger(\boldsymbol{m}, m_t)\rangle . \tag{97}$$

[1]The Λ-2pt function has no disconnected part, for the 3-pt function though, it has to be considered

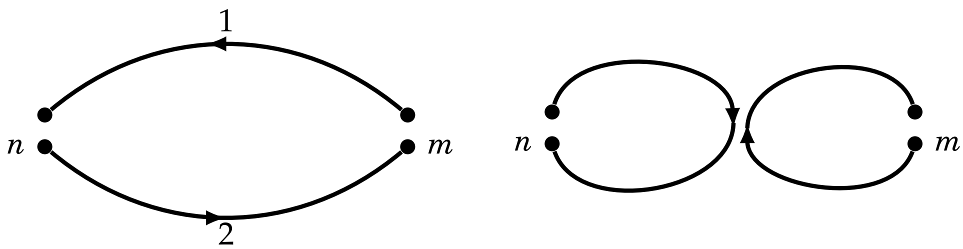


**Figure 9:** Connected (left) and disconnected correlators (right)

It is sufficient to project just one of the two operator to momentum space [13]. So if we fix $m = (\mathbf{0}, m_{t_0})$ the right hand side becomes

$$\sum_{\boldsymbol{n}} e^{-ia\boldsymbol{pn}} \langle O(\boldsymbol{n}, n_t) O^\dagger(\mathbf{0}, m_{t_0}) \rangle . \tag{98}$$

## 2.4 Time evolution in Euclidean time

Using a complete set of energy eigenstates $\mathbb{1} = \sum_n |n\rangle \langle n|$ and the time translation of an operator $O(t) = e^{t\hat{H}} O(0) e^{-t\hat{H}}$, the Euclidean correlator of two operators (eq. (94)) can be written as

$$\left\langle O_2(t) O_1^\dagger(0) \right\rangle = \sum_n \langle 0| e^{t\hat{H}} \hat{O}_2 |n\rangle \langle n| e^{-t\hat{H}} \hat{O}_1^\dagger |0\rangle , \tag{99}$$

where $\hat{H}$ denotes the *Hamiltonion*, which measures the total energy of the system. Applying $\hat{H}$ on an energy eigenstate $|n\rangle$ we get the corresponding eigenvalue equation,

$$\hat{H} |n\rangle = E_n |n\rangle . \tag{100}$$

Considering that the Hamiltonian is hermitian, $H = H^\dagger$, so $\langle n| \hat{H} = \langle n| E_n$ and assuming the translation invariance of the vacuum, $\langle 0| e^{t\hat{H}} = \langle 0|$, we get

$$\left\langle O_2(t) O_1^\dagger(0) \right\rangle = \sum_n \langle 0| \hat{O}_2 |n\rangle \langle n| \hat{O}_1^\dagger |0\rangle e^{-tE_n}. \tag{101}$$

The correlator is a sum of exponentials, which denotes the different energy states of the system. The decay is crucial to interpret lattice results. It shows that the excited state contributions $E_1, E_2, \ldots$ are stronger for small time $t$. To extract the ground states, it is important to look at the correlator at greater time. However, with $smearing$ (see section 2.2), one can reduce the contamination from excited states at earlier times.

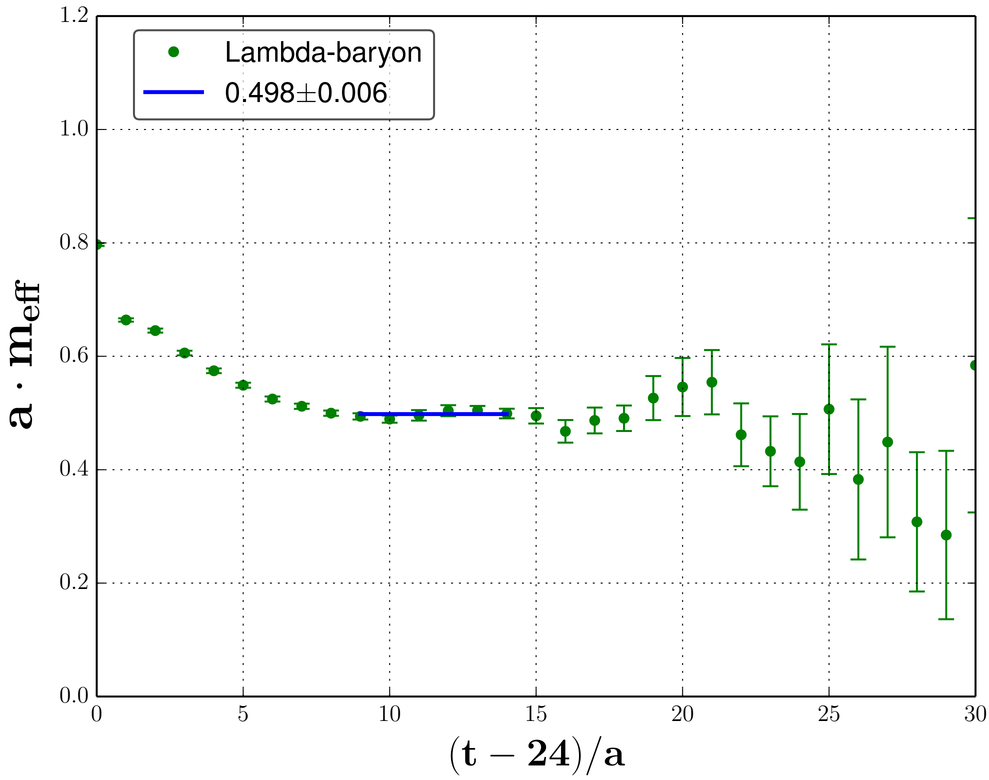


**Figure 10:** Effective mass of $\Lambda$, calculated on H105 at source position $(0,0,0,24)$ with 600 measurments.

## 2.5 The Effective Mass

As mentioned before, the two-point correlator can be written as

$$C_{2pt}(\boldsymbol{p},n_t) = \langle O_B(n_t) O_B^\dagger(0)\rangle = \sum_n \langle 0|\hat{O}_B|n\rangle \langle n|\hat{O}_B^\dagger|0\rangle e^{-tE_n(\boldsymbol{p})} = \sum_n A_n e^{-n_t E_n(\boldsymbol{p})}, \quad (102)$$

with $A_n = |\langle n|\hat{O}_B|0\rangle|^2$ the overlap matrix element of a state created by some baryon operator $\hat{O}_B$ from the vacuum $|0\rangle$ to the $\mathrm{n^{th}}$ energy eigenstate $|n\rangle$. $E_n$ refers to the energy difference relative to the vacuum. Using the two-point function with vanishing momentum $\boldsymbol{p}$, $E_n(\boldsymbol{0}) = m_B$, where $m_B$ is the mass of the baryon, we can extract the effective mass $m_{\text{eff}}$ via the logarithmic ratio

$$am_{\text{eff}}\left(n_t + \frac{1}{2}\right) = \ln\left(\frac{C(\boldsymbol{0},n_t)}{C(\boldsymbol{0},n_t+1)}\right)$$

In figure 10 the effective mass of the $\Lambda$ baryon is shown on the H105 ensemble using a smeared operator at the source and averaging over 600 gauge configurations. The source position was always set at $(0,0,0,24)$ and is therefore shifted left about 24 t for better readability. In the small time region, the excited states affect

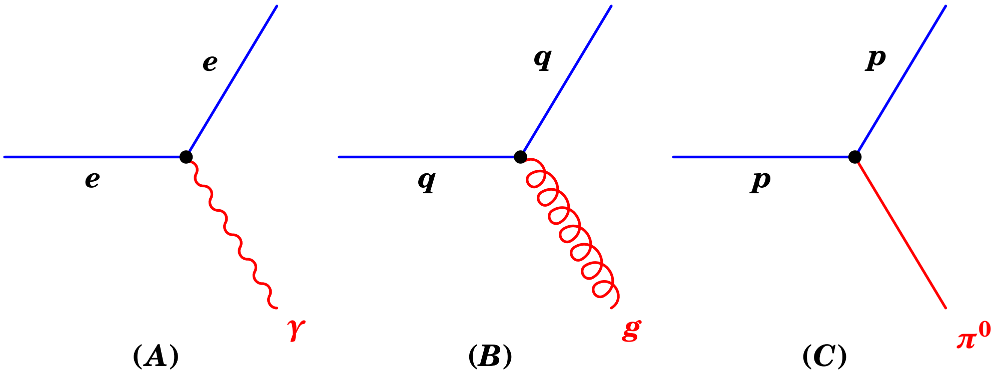


**Figure 11:** (A) Photons $\gamma$ couple to electrons $e$ via the electrical charge. (B) Quarks $q$ are color charged and gluons $g$ couple to them. (C). The axial charge is related to couplings between protons $p$ and pions $\pi^0$. Note: this is the ansatz of an effective theory, which separates (C) from (A) and (B). The axial charge depends on the quark and gluon structure in the proton [36].

the data stronger than at later time. The curve approaches a roughly constant line, the *mass plateau*. Here one can fit a constant to get the mass value

$$am_\Lambda = 0.498 \pm 0.006. \tag{103}$$

The error is calculated using the Jackknife method ( see section 3.1). The errors of the data increase from timeslice 15 onwards. This is due to the bad signal-to-noise ratio of baryons (see section 3.2). To extract particular features of the baryon (like parity, chirality) we use projection a operator $P$ to project them out. We projected the interpolator to positive parity using

$$P = \frac{1}{2}\left(\mathbb{1} + \gamma_0\right).$$

This is done by taking the trace over the Dirac indices of the product of $P$ and $C_2$, hence $\mathrm{Tr}(PC_2)$. The intrinsic parity of the quark is chosen to be positive[1], so the parity of antiquarks is negative. As parity is a multiplicative quantum number [52], the parity of baryons at its ground state is $(+1)^3 = +1$.

## 2.6 The axial charge

We want to discuss the axial charge $g_A$ using the example of the nucleon, as there exist well known experimental values [30]. The axial charge $g_A$ of a baryon contains information on its coupling to the weak interaction. A pictorial representation for 3 different charges is given in figure (2.6). Furthermore the axial charge is related to the axial form factor $G_A$ which contain information about the structure of the nucleon.

[1]This is a convention.

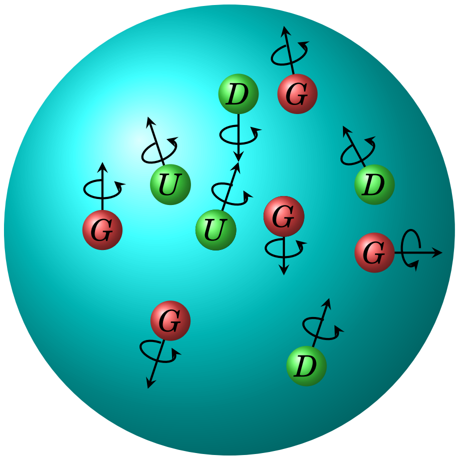


**Figure 12:** Spin distribution of a proton. The red balls are gluons, whereas the green one are quarks.

### 2.6.1 The issue of spin

The proton has a spin of $\frac{1}{2}$. Its constituents, quarks and gluons, have also spins of $\frac{1}{2}$ and 1. If we now consider the orientation of quarks and gluons and the fact that they also can move inside the proton, we have to deal with this additional spin contribution, known as orbital angular momentum. So the spin of the proton is the sum of the spin and orbital angular momentum of quarks and gluons, see figure 12. The axial charge measures the difference of the spin contribution of the up and down quarks to the nucleon spin. The axial charge of the nucleon refers to a coupling $g_A$ between an axial current $A^i_\mu$ and the nucleon,

$$\langle p|A^i_\mu|p\rangle\,, \tag{104}$$

where $A^i_\mu = \overline{\boldsymbol{q}}\gamma_\mu\gamma_5\frac{\lambda^i}{2}\boldsymbol{q}$ is the axial current and $\lambda^i$ the generator of the flavor SU(3). $|p\rangle$ and $\langle p|$ which describe the initial and the final state of a proton can be written as the creation and annihilation operator of the proton $\hat{O}^\dagger_P$ and $\hat{O}_P$ acting on the vacuum $\langle 0|$. With these operators eq. (104) is

$$\langle p|A^i_\mu|p\rangle = \langle 0|\hat{O}_P A^i_\mu \hat{O}^\dagger_P|0\rangle\,. \tag{105}$$

It shows that the axial charge is contained in a three-point function. The coupling can be measured in the $\beta$ decay, in which the neutron transforms to a proton by emitting an electron and an electron antineutrino,

$$n \longrightarrow p + e^- + \overline{\nu}_e.$$

The axial charge is determined experimentally using the beta decay [30] to be

$$g_A = 1.2701 \pm 0.025.$$

On the lattice we use $\lambda^3$ [37], hence

$$\langle p| A_\mu^{u-d} |n\rangle = \langle p| \overline{u}\gamma_\mu\gamma_5 u - \overline{d}\gamma_\mu\gamma_5 d |p\rangle \,. \tag{106}$$

The difference of $u$ and $d$, as mentioned before, is needed to calculate the axial charge of the nucleon. One can choose $\lambda^3$ to avoid quark-disconnected correlators. They vanish in the isospin limit, i.e up-quark mass= down-quark mass.

## 2.7 Calculation of the axial charge of Λ: A theoretical approach

In contrast to the nucleon, we have not enough information about the axial charge of the Λ-baryon from experiment. It has been suggested that the study of polarized Λ baryons may be useful for the study of the nucleon spin structure [38]. With the help of the Cabibbo scheme [39], we will evaluate the axial charge value of the Λ and compare it in a later section with results obtained from the lattice calculation. The matrix element of an octet $I_j$ of currents between two baryon states $B_k$ and $B_i$ can be written as

$$\langle B_i| I_j |B_k\rangle = i f_{ijk} F + d_{ijk} D, \tag{107}$$

with two parameters $F$ and $D$ and the SU(3) structure constants $f_{ijk}$. $d_{ijk}$ can also be build from an anticommutation relation,

$$\{\lambda_i, \lambda_j\} = \frac{4}{3}\delta_{ij}\mathbb{1} + 2 d_{ijk}\lambda_k \tag{108}$$

Under the interchanges of any two indices $f_{ijk}$ is antisymmetric, whereas $d_{ijk}$ is symmetric. All non-zero values are given in table 4. The octet baryons can be build as follows [40]

$$\begin{aligned} p &= \frac{1}{\sqrt{2}}(B_4 + iB_5), & n &= \frac{1}{\sqrt{2}}(B_6 + iB_7), \\ \Sigma\pm &= \frac{1}{\sqrt{2}}(B_1 \pm iB_2), & \Xi^- &= \frac{1}{\sqrt{2}}(B_4 - iB_5), \\ \Xi^0 &= \frac{1}{\sqrt{2}}(B_6 - iB_7), & \Sigma^0 &= B_3, \\ \Lambda &= B_8. \end{aligned}$$

To calculate the isoscalar axial vector charge of the Λ, we use the isoscalar axial

| $ijk$ | $f_{ijk}$ | $ijk$ | $d_{ijk}$ |
|---|---|---|---|
| 123 | 1 | 118 | $\frac{1}{\sqrt{3}}$ |
| 147 | $\frac{1}{2}$ | 146 | $\frac{1}{2}$ |
| 156 | -$\frac{1}{2}$ | 157 | $\frac{1}{2}$ |
| 246 | $\frac{1}{2}$ | 228 | $\frac{1}{\sqrt{3}}$ |
| 257 | $\frac{1}{2}$ | 247 | -$\frac{1}{2}$ |
| 345 | $\frac{1}{2}$ | 256 | $\frac{1}{2}$ |
| 367 | -$\frac{1}{2}$ | 338 | $\frac{1}{\sqrt{3}}$ |
| 458 | $\frac{\sqrt{3}}{2}$ | 344 | $\frac{1}{2}$ |
| 678 | $\frac{\sqrt{3}}{2}$ | 355 | $\frac{1}{2}$ |
| | | 366 | -$\frac{1}{2}$ |
| | | 377 | -$\frac{1}{2}$ |
| | | 448 | -$\frac{1}{2\sqrt{3}}$ |
| | | 558 | -$\frac{1}{2\sqrt{3}}$ |
| | | 668 | -$\frac{1}{2\sqrt{3}}$ |
| | | 778 | -$\frac{1}{2\sqrt{3}}$ |
| | | 888 | $\frac{1}{\sqrt{3}}$ |

**Table 4:** Non-zero values of $f_{ijk}$ and $d_{ijk}$ according to eq. (20) and eq. (108) [40].

vector current

$$I^{iso} = \overline{u}\gamma_\mu\gamma_5 u + \overline{d}\gamma_\mu\gamma_5 d - 2\overline{s}\gamma_\mu\gamma_5 s = \sqrt{3}\cdot\overline{\boldsymbol{q}}\gamma_\mu\gamma_5\lambda^8\boldsymbol{q} = 2\sqrt{3}A^8_\mu,$$

with the base state of flavor SU(3)

$$\boldsymbol{q} = \begin{pmatrix} u \\ d \\ s \end{pmatrix}, \qquad \overline{\boldsymbol{q}} = \begin{pmatrix} \overline{u} & \overline{d} & \overline{s} \end{pmatrix}$$

The factor $\sqrt{3}$ comes from the Gell-Mann matrix $\lambda^8$. Replacing $I_j$ by $I^{\text{iso}}$ in eq. (107), we get

$$\langle B_8|2\sqrt{3}A^8_\mu|B_8\rangle = 2\sqrt{3}(if_{888}F + d_{888}D) = -2D. \tag{109}$$

with the values from table 4. This axial vector term corresponds to the axial charge $g_A$ [40]. From the strangeness-conserving decay [41]

$$\Sigma\pm \rightarrow \Lambda e^\pm \nu_e$$

one get the experimental value $g_{A,\Sigma\Lambda}$ with the parameter $\sqrt{\frac{2}{3}}D \sim 0.62$. Inserting it in eq. (109) we get the estimate

$$g_A \sim -1.52.$$

We have to consider, that this approach is using the exact SU(3) symmetry. In the lattice calculation however this symmetry is broken. The value should only be used as an orientation.

## 2.8 Calculation of axial charge of Λ on the lattice

The following derivation is motivated by Harvey B. Meyer's notes about the nucleon form factor [42]. We will throughout this measurement be using continuum coordinates $x$ and $y$ to get the result analytically. In the previous section we mentioned that the axial charge is contained in the three-point function. Here we want to show how to extract it from the lattice calculation. To calculate the axial charge of the Λ-baryon on the lattice, we consider the following ratio of three-point and two-point functions as suggested in [54]

$$R_I(x_0, y_0, \boldsymbol{q}) = \frac{C_{3,I}(x_0, y_0, \boldsymbol{q})}{C_2(x_0, \boldsymbol{0})} \cdot \sqrt{\frac{C_2(y_0 - x_0, \boldsymbol{q}) C_2(y_0, \boldsymbol{0}) C_2(x_0, \boldsymbol{0})}{C_2(y_0 - x_0, \boldsymbol{0}) C_2(y_0, \boldsymbol{q}) C_2(x_0, \boldsymbol{q})}}, \tag{110}$$

with $I$ the insertion operator between two baryon states. The operator is inserted at time $y_0$ and the sink is located at time $x_0$. With the ratio we get rid of the time and energy dependence. Also the coupling constant $Z_B$, which appears in the following calculation, will cancel. We will project the correlators using the projector

$$P = \frac{1}{2}(1 + \gamma_0^E)(1 + i\gamma_5^E \gamma_3^E), \tag{111}$$

where $\gamma_\mu^E$ indicates the Dirac-matrices in Euclidean space (see A.1).

### 2.8.1 Axial charge: Two-point correlator

We start by evaluating the two-point function in momentum space (see eq.(98)),

$$C_2^{\alpha\beta}(x_0, \boldsymbol{p}) = \int d^3x e^{-i\boldsymbol{p}\boldsymbol{x}} \langle 0 | \hat{O}_\alpha(x) \hat{O}_\beta^\dagger(0) | 0 \rangle \,. \tag{112}$$

$\alpha$ is the Dirac index and $\hat{O}$ the interpolating operator. With the help of the completeness relation

$$\mathbb{1} = \int \frac{d^3p'}{(2\pi)^3 2E_{\boldsymbol{p}'}} \sum_{s'} |B(p',s')\rangle \langle B(p',s')|, \tag{113}$$

where B(p′,s′) represents a baryon with momemtum p′ and spin s′, and the translation operator, $O(x) = e^{i\hat{p}x}O(0)e^{-i\hat{p}x}$, we get

$$C_2^{\alpha\beta}(x_0,\boldsymbol{p}) = \int d^3x e^{-i\boldsymbol{p}\boldsymbol{x}} \int \frac{d^3p'}{(2\pi)^3 2E_{\boldsymbol{p}'}} \sum_{s'} \langle 0|\hat{O}_\alpha(0)|B(p',s')\rangle\, e^{-ip'x} \langle B(p',s')|\hat{O}^\dagger_\beta(0)|0\rangle\,. \tag{114}$$

We assume translation invariance of the vacuum, so that $\langle 0|e^{i\hat{p}x} = \langle 0|$ holds. The overlap matrix elements can be expressed as

$$\begin{aligned} \langle 0|\hat{O}_\alpha(0)|B(p',s')\rangle &= Z_B u^{s'}_\alpha(p'), \\ \langle B(p',s')|\hat{O}^\dagger_\beta(0)|0\rangle &= Z^*_B \bar{u}^{s'}_\beta(p'), \end{aligned} \tag{115}$$

where $u^{s'}(p')$ are the plane-wave solutions for baryons of the Dirac equation, and $Z_B$ is a coupling strength of $O(0)$ to the state $|B(p',s')\rangle$. With the overlaps we get

$$C_2^{\alpha\beta} = |Z_B|^2 \int \frac{d^3p'}{(2\pi)^3 2E_{\boldsymbol{p}'}} e^{-iE_{\boldsymbol{p}'}x_0} \int d^3x e^{-i(\boldsymbol{p}-\boldsymbol{p}')\boldsymbol{x}} \sum_{s'} u^{s'}_\alpha(p')\bar{u}^{s'}_\beta(p')$$

where we used $e^{-ip'x}$=$e^{-i(E_{\boldsymbol{p}'}x_0-\boldsymbol{p}'\boldsymbol{x})}$. The spinors are now summed over the spin (see in [8] eq. 3.66),

$$\sum_{s'} u^{s'}_\alpha(p')\bar{u}^{s'}_\beta(p') = (E_{\boldsymbol{p}'}\gamma^E_0 + i\boldsymbol{p}'\boldsymbol{\gamma}^{\boldsymbol{E}} + m)\alpha\beta. \tag{116}$$

With a Wick rotation $x_0 \longrightarrow -ix_0$ the two-point correlator is then,

$$C_2^{\alpha\beta}(x_0,\boldsymbol{p}) = |Z_B|^2 \frac{e^{-E_{\boldsymbol{p}}x_0}}{2E_{\boldsymbol{p}}} (E_{\boldsymbol{p}}\gamma^E_0 + i\boldsymbol{p}\boldsymbol{\gamma}^{\boldsymbol{E}} + m)_{\alpha\beta}. \tag{117}$$

Consider the Euclidean gamma matrices, that causes a sign change of the term $\boldsymbol{ip\gamma^E}$. As mentioned before we project the correlator using $P$ in eq. (111)

$$
\begin{aligned}
\tilde{C}_2(x_0,\boldsymbol{p}) =& \mathrm{Tr}[PC_2(x_0,\boldsymbol{p})] \\
=& \mathrm{Tr}\left[\frac{1}{2}(1+\gamma_0^E)(1+i\gamma_5^E\gamma_3^E)|Z_B|^2\frac{e^{-E_{\boldsymbol{p}}x_0}}{2E_{\boldsymbol{p}}}(E_{\boldsymbol{p}}\gamma_0^E+\boldsymbol{ip\gamma^E}+m)\right] \\
=& \frac{1}{2}|Z_B|^2\frac{e^{-E_{\boldsymbol{p}}x_0}}{2E_{\boldsymbol{p}}}\mathrm{Tr}\Big[E_{\boldsymbol{p}}\gamma_0^E+\boldsymbol{ip\gamma^E}+m+i\gamma_5^E\gamma_3^E E_{\boldsymbol{p}}\gamma_0^E-\gamma_5^E\gamma_3^E\boldsymbol{p\gamma^E} \\
&+i\gamma_5^E\gamma_3^E m+E_{\boldsymbol{p}}+i\gamma_0^E\boldsymbol{p\gamma^E}-\gamma_0^E m+i\gamma_0^E\gamma_5^E\gamma_3^E E_{\boldsymbol{p}}\gamma_0^E+\gamma_5^E\gamma_3^E\boldsymbol{p\gamma_0^E} \\
&+i\gamma_0^E\gamma_5^E\gamma_3^E m\Big].
\end{aligned}
$$

With $\mathrm{Tr}[m]=4m$ and $\mathrm{Tr}[E_{\boldsymbol{p}}]=4E_{\boldsymbol{p}}$, since they are diagonal matrices, and Tr[remains]=0 we get

$$
\tilde{C}_2(x_0,\boldsymbol{p}) = |Z_B|^2\Big(\frac{m}{E_{\boldsymbol{p}}}+1\Big)e^{-E_{\boldsymbol{p}}x_0}. \tag{118}
$$

### 2.8.2 Axial charge: Three-point correlator

A general current is defined as a quark bilinear

$$
I=\bar{\psi}\Gamma\psi. \tag{119}
$$

To calculate the axial vector charge, we choose an axial vector current, so

$$
\Gamma=\gamma^\mu\gamma^5 \tag{120}
$$

hence we rename the current

$$
I=A_M^\mu
$$

with $A_M^\mu$ the axial current in Minkowski space. According to [43] the following relation for the matrix element of the axial vector current can be used in the isospin limit

$$
\langle B(p',s')|A_M^\mu(x)|B(p,s)\rangle = e^{iqx}\bar{u}^{s'}(p')\underbrace{\Big(\gamma^\mu\gamma^5G_A(q^2)+\gamma^5\frac{q^\mu}{2m}G_P(q^2)\Big)}_{\mathscr{A}(q)}u^s(p),
$$

where $q$=$p'-p$ is the momentum transfer and $|B\rangle$ an octet baryon state. $G_A$ is the axial form factor and $G_P$ the pseudo-scalar form factor. The axial charge is defined as the axial form factor at zero momentum transfer, i.e.

$$G_A(0) = g_A.$$

If we calculate the three-point correlator with zero momentum in the final state and in the spectral representation (inserting the completeness relation) we obtain [42]

$$\begin{aligned} C_3^{\alpha\beta}(x_0, y_0, \boldsymbol{q}) &= \int d^3y \int d^3x e^{i\boldsymbol{q}\boldsymbol{y}} \langle 0|\hat{O}_\alpha(x)A(y)\hat{O}^\dagger_\beta(0)|0\rangle \\ &= |Z_B|^2 \frac{e^{-E_{\boldsymbol{q}}y_0}}{2E_{\boldsymbol{q}}} \frac{e^{-m(x_0-y_0)}}{2m} \big((m\gamma_0^E + m)\mathscr{A}(q)(E_{\boldsymbol{q}}\gamma_0^E + i\boldsymbol{q}\boldsymbol{\gamma}^E + m)\big), \end{aligned} \tag{121}$$

where we also summed over the spins. With the $P$ defined in eq. (111), the projected three-point correlator takes the form

$$\tilde{C}_3(x_0, y_0, \boldsymbol{q}) = \mathrm{Tr}\big[PC_3(x_0, y_0, \boldsymbol{q})\big] = |Z_B|^2 \frac{e^{-E_{\boldsymbol{q}}y_0}}{2E_{\boldsymbol{q}}} \frac{e^{-m(x_0-y_0)}}{2m} \cdot T_{A^\mu_M}. \tag{122}$$

Two cases are possible for $T_{A^\mu_M}$,

$$T_{A^\mu_M} = \begin{cases} 4mq_3\big(G_A(q^2) + \frac{q^0}{2m}G_P(q^2)\big), & \mu = 0, \\ -4m\big(G_A(q^2)(m + E_{\boldsymbol{q}})\delta_{3k} - \frac{q_3 q_k}{2m}G_P(q^2)\big), & \mu = k, \end{cases}$$

in which we used that

$$\mathrm{Tr}\left[\gamma_3^E \gamma_k^E\right] = 4\delta_{3k}. \tag{123}$$

To extract $g_A$ we choose $\mu = 3$, the current in Euclidean space $A^3_E = -iA^3_M$ and $q = 0$, hence eq. (122) takes the form

$$\tilde{C}_3(x_0, y_0, \boldsymbol{q}) = 2ie^{-mx_0}G_A(0) \tag{124}$$

The ratio eq. (110) reduces to

$$R_{A^3_E}(x_0, y_0, \boldsymbol{0}) = \frac{\tilde{C}_{3,A^3_E}(x_0, y_0, \boldsymbol{0})}{\tilde{C}_2(x_0, \boldsymbol{0})} \tag{125}$$

Thus we get

$$g_A = G_A(0) = \mathrm{Im}(R_{A_E^3}(x_0, y_0, \mathbf{0})). \tag{126}$$

# 3 Error estimation

Reliable estimates of errors demand a large set of measurements. There is a high computational effort to do the measurements, in our case the generation of gauge field configurations and to evaluate the high dimensional sum (see eq. (81)). Hence, we have to make use of estimators. Resampling methods are used to estimate the precision of sample statistic with correlated data. Standard method for calculating errors are impractical, when the analysis is more involved[1]. The so-called Jackknife and Bootstrap method provides us with an method for determining the propagation of errors. In the following section we show how to deal with data using the Jackknife method and why errors increase with larger time. Informations about the Bootstrap method is given in [46].

## 3.1 Jackknife

Suppose we have a data vector $\boldsymbol{X}$ with $N$ data points [47]

$$\boldsymbol{X} = (X_1, X_2, \ldots, X_{N-1}, X_N). \tag{127}$$

The data vector has been generated via a Monte Carlo procedure , i. e. $X_n$ has been computed on a number of configurations along a Markov chain. Furthermore, $\boldsymbol{X}$ is not a population but a sample, since we generated a finite amount of gauge configurations. The mean of the sample is defined as

$$\overline{X} = \frac{1}{N} \sum_{n=1}^{N} X_n.$$

As we are averaging over a data sample, our observable tends to be higher or lower than the true value[2]. The difference between the true value and the sample means is called *bias*. To calculate the *unbiased* estimation of the standard deviation of the sample mean we use

$$\sigma_{\overline{X}} = \frac{\sigma}{\sqrt{N}} = \sqrt{\frac{1}{N(N-1)} \sum_{n=1}^{N} (X_n - \overline{X})^2}. \tag{128}$$

Consider the factor $\frac{1}{N-1}$, which is referred to as *Bessel's correction* [48]. But this error formulation gets impractical when applying it on a observable Q, which can be a difficult function of the raw data or resulting from a fit ( error propagation). Here the Jackknife method comes into play. Suppose we have now an observable $\boldsymbol{Q}$, calculated from the original sample $\boldsymbol{X}$. The Jackknife begins with creating

[1] the axial charge e.g. has in matters of raw data a complex structure. It is the ratio of 2- and 3-point functions which also themselves have inner mathematical structure see section 2.5.

[2] True value denotes here the average over the population.

subsets of the data vector $\boldsymbol{X}$ by removing the $i$th entry, hence we get

$$\boldsymbol{X}_{[i]} = (X_1, X_2, \ldots, X_{i-1}, X_{i+1}, \ldots, X_{N-1}, X_N). \tag{129}$$

From each subset $\boldsymbol{X}_{[i]}$ one determines the observable $Q_{J_i}$. Then the Jackknife error is defined as [13]

$$\sigma_J = \sqrt{\frac{N-1}{N}\sum_{i=1}^{N}\left(Q_{J_i} - Q\right)^2}. \tag{130}$$

To see how the Jackknife works, we want to compute error of the sample $\boldsymbol{X}$ with the Jackknife method. We know how to calculate this error with the standard method. The Jackknife method computes the Jackknife sample means

$$X_{J_i} = \frac{1}{N-1}\sum_{n=1}^{N-1} X_{[i]_n}, \tag{131}$$

then the Jackknife error in the mean reads

$$\sigma_{J_X} = \sqrt{\frac{N-1}{N}\sum_{i=1}^{N}\left(X_{J_i} - \overline{X}\right)^2}, \tag{132}$$

comparing eq. (132) und eq. (128), we see that the factor $N-1$ is in the numerator rather the denominator. We get equality if

$$X_{J_i} - \overline{X} = \frac{1}{N-1}\left(\overline{X} - X_n\right) \tag{133}$$

holds. Evaluating $X_{J_i} - \overline{X}$ we get,

$$
\begin{aligned}
X_{J_i} - \overline{X} &= \sum_{n \neq i} X_n - \frac{1}{N} \sum_n X_n \\
&= \frac{N \sum_{n \neq i} X_n - (N-1) \sum_n X_n}{N(N-1)} \\
&= \frac{N \sum_{n \neq i} X_n - (N-1) \left( \sum_{n \neq i} X_n + X_i \right)}{N(N-1)} \\
&= \frac{\frac{1}{N} \sum_{n \neq i} X_n - X_i + \frac{1}{N} X_i}{N-1} \\
&= \frac{\frac{1}{N} \sum_n X_n - X_i}{N-1} \\
&= \frac{1}{N} \left( \overline{X} - X_i \right).
\end{aligned}
\tag{134}
$$

Thus in the case of the sample mean, the Jackknife error reduces to the standard formula.

## 3.2 Signal-to-noise ratio

Looking at figure 10 in chapter 2, we see that the noise grows with larger t. The noise problem arises from the fact that particles described by a given interpolator can decay into lighter particles, which have the same quantum numbers, due to the kinematics of a considered ensemble. The signal-to-noise ratio is defined as

$$
R_{NS} = \frac{\langle C_2 \rangle}{\sigma^2} \tag{135}
$$

The expectation value of the $\Lambda$ two-point correlation function is $\langle C_2 \rangle \sim e^{-m_\Lambda t}$. The variance can be estimated as [51]

$$
\sigma^2 \sim \left\langle \left| C_2 \right|^2 \right\rangle - |\langle C_2 \rangle|^2 \sim e^{-(2m_\pi + m_\phi)t}.
$$

The $\Lambda$ two-point function is obtained from the contraction of the 3 quarks u, d, s with the anti-quarks $\overline{u}, \overline{d}, \overline{s}$. They can be combined to two $\pi$-mesons and one $\phi$-meson. The signal-to-noise ratio is then

$$
R_{SN} \sim e^{-\left(m_\lambda - (m_\pi + \frac{1}{2} m_\phi)\right)t}.
$$

Thus it falls with larger $t$ since $m_\Lambda - (m_\pi + \frac{1}{2} m_\phi) > 0$. In figure 13 we show how $R_{SN}$ evolves with $t$. We see an exponential decay of $R_{SN}$, as estimated in our formula, but the calculation of the exponent remains.

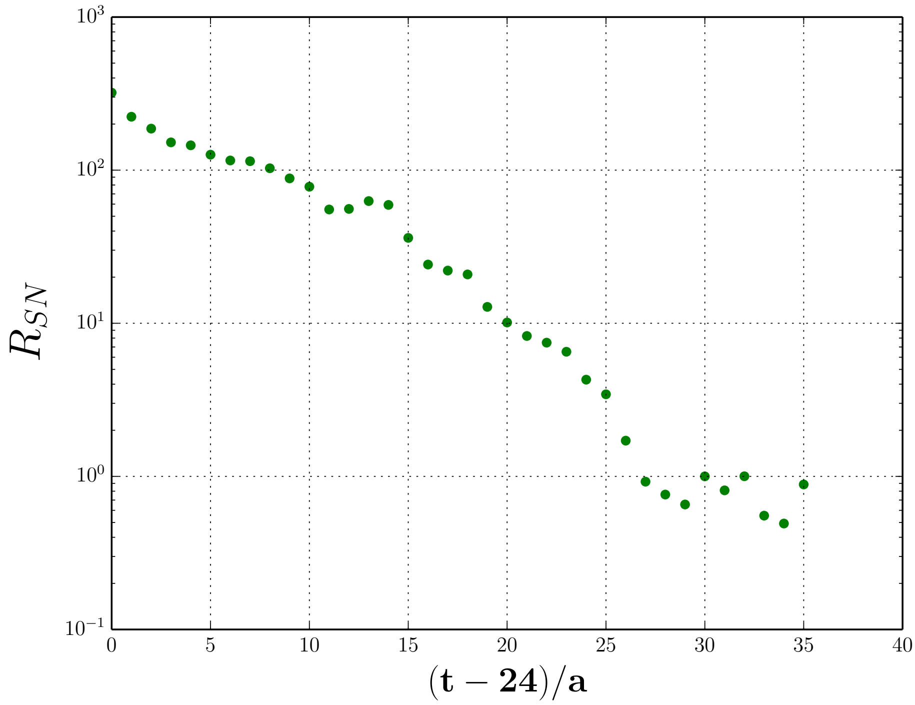


**Figure 13:** Signal-to-noise ratio on the log scale plotted against time $t$. Our estimation can be confirmed due to the roughly linear trend.

# 4 Calculation on the Lattice

Now that we know how to use Wick contractions to calculate fermionic expectation values and how to interpret the results on the hadronic level, we want to use this knowledge to analyze the $\Lambda$-baryon, which is a member of the SU(3) octet.

## 4.1 $\Lambda$ Two-point correlator

The $\Lambda$-baryon consists of an up-, a down-, and a strange quark and has a mass of roughly 1116 MeV [30]. It has strangeness S=-1 and a charge of Q=0. $\Lambda$ is part of the baryon octet and is an isosinglet particle (figure 14). We can build the $\Lambda$ interpolator as

$$\Lambda = \epsilon_{abc} u_\gamma^a \left( d_\alpha^b (C\gamma_5)_{\alpha\beta} s_\beta^c \right), \tag{136}$$

where $C$ is the charge conjugation matrix,

$$\psi(x) \xrightarrow{C} \psi(n)^C = C^{-1}\overline{\psi}(n)^T, \qquad \overline{\psi}(n) \xrightarrow{C} \overline{\psi}(x)^C = -\psi(n)^T C. \tag{137}$$

Acting on the Dirac indices, we obtain

$$C\gamma_\mu C^{-1} = -\gamma_\mu^T, \qquad C = i\gamma_0\gamma_2. \tag{138}$$

The convention used in this thesis for the Dirac matrices can be found in appendix A.1. The epsilon tensor secures the invariance under color transformations. The color state of a baryon can be written as[1] [33]

$$|B\rangle_c = \epsilon_{ijk}\chi^i \otimes \chi^j \otimes \chi^k, \tag{139}$$

where $\chi^i$ is a basis of a complex Hilbert space. The SU(3)-color transformation is

$$\begin{aligned} |B\rangle_c \longmapsto |B'\rangle_c &= \epsilon_{ijk}\left(U\chi^i\right) \otimes \left(U\chi^j\right) \otimes \left(U\chi^k\right) \\ &= \epsilon_{ijk} U_a^i U_b^j U_c^k \chi^a \otimes \chi^b \otimes \chi^c \end{aligned}. \tag{140}$$

[1] We omitted the normalization factor for simplicity.

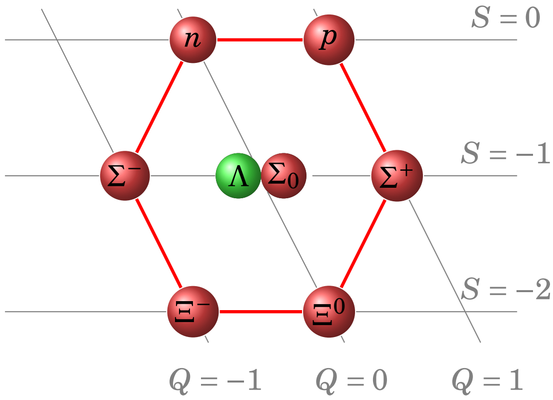


**Figure 14:** The baryon octet, $\Sigma_0$ has I=1, whereas $\Lambda$ is a Isospin singlet I=0

For a 3×3-matrix $M$ with the entries $m_{ij}$, the determinant is given by

$$\det(M) = \epsilon_{ijk} m_{1i} m_{2j} m_{3k}. \tag{141}$$

Using this definition we can evaluate $\epsilon_{ijk} U_a^i U_b^j U_c^k$

- for $abc = 123$ (*and all other even permutations*), $\epsilon_{ijk} U_1^i U_2^j U_3^k$ = det(U) = 1,
- for $abc = 213$ (*and all other odd permutations*), $\epsilon_{ijk} U_2^i U_1^j U_3^k$ = -$\epsilon_{jik} U_1^j U_2^i U_3^k$= -det(U) = $-1$,
- otherwise, $\epsilon_{ijk} U_a^i U_b^j U_c^k = 0$.

This leads us to the result $\epsilon_{ijk} U_a^i U_b^j U_c^k$ =$\epsilon_{abc}$ and shows that the interpolator is color invariant. Going back to eq. (136), the parentheses, where $d$ and $s$ are contracted with $C$, form a so-called *diquark*. The diquark model is used for the calculation of baryon masses. The quantum number of the $\Lambda$-baryon can also be obtained with different diquark structures. For this thesis we use a more general interpolator for $\Lambda$. According to Gattringer and Lang [13] the $\Lambda$ interpolator reads:

$$\Lambda_\gamma = \epsilon_{abc}\Big(2 s_\gamma^a u_\beta^b (C\gamma_5)_{\beta\alpha} d_\alpha^c + d_\gamma^a u_\beta^b (C\gamma_5)_{\beta\alpha} s_\alpha^c - u_\gamma^a d_\beta^b (C\gamma_5)_{\beta\alpha} s_\alpha^c\Big),$$
$$\overline{\Lambda}_\gamma = \epsilon_{abc}\Big(2 \overline{u}_\alpha^a (C\gamma_5)_{\alpha\beta} \overline{d}_\beta^b \overline{s}_\gamma^c + \overline{u}_\alpha^a (C\gamma_5)_{\alpha\beta} \overline{s}_\beta^b \overline{d}_\gamma^c - \overline{d}_\gamma^a (C\gamma_5)_{\alpha\beta} \overline{s}_\beta^b \overline{u}_\gamma^c\Big).$$

Notice the open Dirac indices, they will be used to project the correlator to the suitable symmetry via the trace. To calculate the mass we projected, as mentioned before, the interpolator to positive parity. For the calculation of the axial charge we projected it with a $P$ defined in eq. (111). The two point-correlator can be

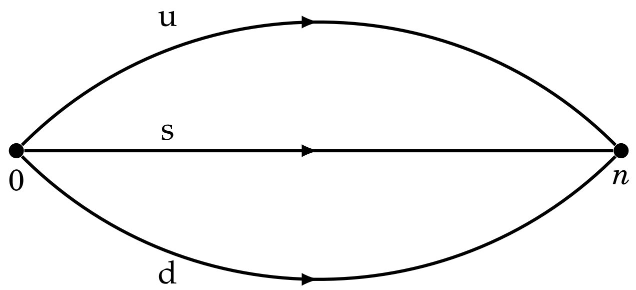


**Figure 15:** Pictorial representation of the two-point function. Λ is created at 0 and annihilated at n.

obtained through

$$P_{\gamma'\gamma}\langle\Lambda_\gamma(n)\overline{\Lambda}_{\gamma'}(0)\rangle =$$
$$P_{\gamma'\gamma}\Big[\epsilon_{abc}\Big(\langle 2s(n)^a_\gamma u(n)^b_\beta(C\gamma_5)_{\beta\alpha}d(n)^c_\alpha\rangle + \langle d(n)^a_\gamma u(n)^b_\beta(C\gamma_5)_{\beta\alpha}s(n)^c_\alpha\rangle -$$
$$\langle u(n)^a_\gamma d(n)^b_\beta(C\gamma_5)_{\beta\alpha}s(n)^c_\alpha\rangle\Big)$$
$$\cdot\epsilon_{a'b'c'}\Big(\langle 2\overline{u}(0)^{a'}_{\alpha'}(C\gamma_5)_{\alpha'\beta'}\overline{d}(0)^{b'}_{\beta'}\overline{s}(0)^{c'}_{\gamma'}\rangle + \langle\overline{u}(0)^{a'}_{\alpha'}(C\gamma_5)_{\alpha'\beta'}\overline{s}(0)^{b'}_{\beta'}\overline{d}(0)^{c'}_{\gamma'}\rangle -$$
$$\langle\overline{d}(0)^{a'}_{\gamma'}(C\gamma_5)_{\alpha'\beta'}\overline{s}(0)^{b'}_{\beta'}\overline{u}(0)^{c'}_{\gamma'}\rangle\Big)\Big].$$

The baryon is created at space-time point 0 and annihilated at $n$. A pictorial representation is given in figure 15. Now we factor out

$$P_{\gamma'\gamma}\langle\Lambda_\gamma(n)\overline{\Lambda}_{\gamma'}(0)\rangle = P_{\gamma'\gamma}\epsilon_{abc}\epsilon_{a'b'c'}$$
$$\Big(\langle 4s(n)^a_\gamma u(n)^b_\beta(C\gamma_5)_{\beta\alpha}d(n)^c_\alpha\overline{u}(0)^{a'}_{\alpha'}(C\gamma_5)_{\alpha'\beta'}\overline{d}(0)^{b'}_{\beta'}\overline{s}(0)^{c'}_{\gamma'}\rangle +$$
$$\langle 2s(n)^a_\gamma u(n)^b_\beta(C\gamma_5)_{\beta\alpha}d(n)^c_\alpha\overline{u}(0)^{a'}_{\alpha'}(C\gamma_5)_{\alpha'\beta'}\overline{s}(0)^{b'}_{\beta'}\overline{d}(0)^{c'}_{\gamma'}\rangle -$$
$$\langle 2s(n)^a_\gamma u(n)^b_\beta(C\gamma_5)_{\beta\alpha}d(n)^c_\alpha\overline{d}(0)^{a'}_{\alpha'}(C\gamma_5)_{\alpha'\beta'}\overline{s}(0)^{b'}_{\beta'}\overline{u}(0)^{c'}_{\gamma'}\rangle +$$
$$\langle 2d(n)^a_\gamma u(n)^b_\beta(C\gamma_5)_{\beta\alpha}s(n)^c_\alpha\overline{u}(0)^{a'}_{\alpha'}(C\gamma_5)_{\alpha'\beta'}\overline{d}(0)^{b'}_{\beta'}\overline{s}(0)^{c'}_{\gamma'}\rangle +$$
$$\langle d(n)^a_\gamma u(n)^b_\beta(C\gamma_5)_{\beta\alpha}s(n)^c_\alpha\overline{u}(0)^{a'}_{\alpha'}(C\gamma_5)_{\alpha'\beta'}\overline{s}(0)^{b'}_{\beta'}\overline{d}(0)^{c'}_{\gamma'}\rangle -$$
$$\langle d(n)^a_\gamma u(n)^b_\beta(C\gamma_5)_{\beta\alpha}s(n)^c_\alpha\overline{d}(0)^{a'}_{\alpha'}(C\gamma_5)_{\alpha'\beta'}\overline{s}(0)^{b'}_{\beta'}\overline{u}(0)^{c'}_{\gamma'}\rangle -$$
$$\langle 2u(n)^a_\gamma d(n)^b_\beta(C\gamma_5)_{\beta\alpha}s(n)^c_\alpha\overline{u}(0)^{a'}_{\alpha'}(C\gamma_5)_{\alpha'\beta'}\overline{d}(0)^{b'}_{\beta'}\overline{s}(0)^{c'}_{\gamma'}\rangle -$$
$$\langle u(n)^a_\gamma d(n)^b_\beta(C\gamma_5)_{\beta\alpha}s(n)^c_\alpha\overline{u}(0)^{a'}_{\alpha'}(C\gamma_5)_{\alpha'\beta'}\overline{s}(0)^{b'}_{\beta'}\overline{d}(0)^{c'}_{\gamma'}\rangle +$$
$$\langle u(n)^a_\gamma d(n)^b_\beta(C\gamma_5)_{\beta\alpha}s(n)^c_\alpha\overline{d}(0)^{a'}_{\alpha'}(C\gamma_5)_{\alpha'\beta'}\overline{s}(0)^{b'}_{\beta'}\overline{u}(0)^{c'}_{\gamma'}\rangle\Big).$$

With the contraction $\langle f(n)^a_\alpha\overline{f}(0)^b_\beta\rangle = F(n,0)^{ab}_{\alpha\beta}$ we get $U$, $D$ and $S$, which denotes the propagators of the u-, d-, and s-quarks

$$
\begin{aligned}
&P_{\gamma'\gamma}\langle\Lambda_\gamma(n)\overline{\Lambda}_{\gamma'}(0)\rangle = P_{\gamma'\gamma}\epsilon_{abc}\epsilon_{a'b'c'}\\
&\Big(-4S(n,0)^{ac'}_{\gamma\gamma'}U(n,0)^{ba'}_{\beta\alpha'}(C\gamma_5)_{\beta\alpha}D(n,0)^{cb'}_{\alpha\beta'}(C\gamma_5)_{\alpha'\beta'}+\\
&2S(n,0)^{ab'}_{\gamma\beta'}U(n,0)^{ba'}_{\beta\alpha'}(C\gamma_5)_{\beta\alpha}D(n,0)^{cc'}_{\alpha\gamma'}(C\gamma_5)_{\alpha'\beta'}+\\
&2S(n,0)^{ab'}_{\gamma\beta'}U(n,0)^{bc'}_{\beta\gamma'}(C\gamma_5)_{\beta\alpha}D(n,0)^{cb'}_{\alpha\alpha'}(C\gamma_5)_{\alpha'\beta'}+\\
&2D(n,0)^{ab'}_{\gamma\beta'}U(n,0)^{ba'}_{\beta\alpha'}(C\gamma_5)_{\beta\alpha}S(n,0)^{cc'}_{\alpha\gamma'}(C\gamma_5)_{\alpha'\beta'}-\\
&D(n,0)^{ac'}_{\gamma\gamma'}U(n,0)^{ba'}_{\beta\alpha'}(C\gamma_5)_{\beta\alpha}S(n,0)^{cb'}_{\alpha\beta'}(C\gamma_5)_{\alpha'\beta'}-\\
&D(n,0)^{aa'}_{\gamma\alpha'}U(n,0)^{bc'}_{\beta\gamma'}(C\gamma_5)_{\beta\alpha}S(n,0)^{cb'}_{\alpha\beta'}(C\gamma_5)_{\alpha'\beta'}+\\
&2U(n,0)^{aa'}_{\gamma\alpha'}D(n,0)^{bb'}_{\beta\beta'}(C\gamma_5)_{\beta\alpha}S(n,0)^{cc'}_{\alpha\gamma'}(C\gamma_5)_{\alpha'\beta'}-\\
&U(n,0)^{aa'}_{\gamma\alpha'}D(n,0)^{bc'}_{\beta\gamma'}(C\gamma_5)_{\beta\alpha}S(n,0)^{cb'}_{\alpha\beta'}(C\gamma_5)_{\alpha'\beta'}-\\
&U(n,0)^{ac'}_{\gamma\gamma'}D(n,0)^{ba'}_{\beta\alpha'}(C\gamma_5)_{\beta\alpha}S(n,0)^{cb'}_{\alpha\beta'}(C\gamma_5)_{\alpha'\beta'}\Big).
\end{aligned}
$$

The sign changes are due to the anti-commutation of Grassmann variables. In the next step we contract $C\gamma_5$ and use $C\gamma_5 = \Gamma^B$:

$$
\begin{aligned}
&P_{\gamma'\gamma}\langle\Lambda_\gamma(n)\overline{\Lambda}_{\gamma'}(0)\rangle = P_{\gamma'\gamma}\epsilon_{abc}\epsilon_{a'b'c'}\\
&(-4S^{ac'}_{\gamma\gamma'}U^{ba'}_{\beta\alpha'}(\Gamma^B D\Gamma^{B,T})^{cb'}_{\beta\alpha'}+2S^{ab'}_{\gamma\beta'}(\Gamma^{B,T}U\Gamma^B)^{ba'}_{\alpha\beta'}D^{cc'}_{\alpha\gamma'}+\\
&2S^{ab'}_{\gamma\beta'}U^{bc'}_{\beta\gamma'}(\Gamma^B D\Gamma^B)^{ca'}_{\beta\beta'}+2D^{ab'}_{\gamma\beta'}(\Gamma^{B,T}U\Gamma^B)_{\alpha\beta'}S^{cc'}_{\alpha\gamma'}-\\
&D^{ac'}_{\gamma\gamma'}(\Gamma^{B,T}U\Gamma^B)^{ba'}_{\alpha\beta'}S^{cb'}_{\alpha\beta'}-D^{aa'}_{\gamma\alpha'}U^{bc'}_{\beta\gamma'}(\Gamma^B S\Gamma^{B,T})^{cb'}_{\beta\alpha'}+\\
&2U^{aa'}_{\gamma\alpha'}(\Gamma^{B,T}D\Gamma^{B,T})^{bb'}_{\alpha\alpha'}S^{cc'}_{\alpha\gamma'}-U^{aa'}_{\gamma\alpha'}D^{bc'}_{\beta\gamma'}(\Gamma^B S\Gamma^{B,T})^{cb'}_{\beta\alpha'}-\\
&U^{ac'}_{\gamma\gamma'}(\Gamma^{B,T}D\Gamma^B)^{ba'}_{\alpha\beta'}S^{cb'}_{\alpha\beta'}),
\end{aligned}
$$

where $\Gamma^{B,T}$ is the transposed $\Gamma^B$. Now we contract $P_{\gamma'\gamma}$ and we use the QDP[1] operator 'quarkContract' (see QDP Manual [31] ) which also includes a color con-

[1]QDP is an application which is included in the openQCD package. It provides parallel operations on all lattice sites. We are also using its operator Syntax.

traction,

$$
\begin{aligned}
P_{\gamma'\gamma}\langle\Lambda_\gamma(n)\overline{\Lambda}_{\gamma'}(0)\rangle = &-4(PS)^{ac'}_{\gamma'\gamma'}\text{quarkContract13}(U,\Gamma^B D\Gamma^{B,T})^{c'a}_{\alpha'\alpha'}\\
&-2(PS)^{ab'}_{\gamma'\beta'}\text{quarkContract13}(\Gamma^{B,T}U\Gamma^B,D)^{b'a}_{\beta'\gamma'}\\
&+2(PS)^{ab'}_{\gamma'\beta'}\text{quarkContract13}(U,(\Gamma^B D\Gamma^B))^{b'a'}_{\gamma'\beta'}\\
&-2(PD)^{ab'}_{\gamma'\beta'}\text{quarkContract13}(\Gamma^{B,T}U\Gamma^B,S)^{b'a}_{\beta'\gamma'}\\
&-(PD)^{ac'}_{\gamma'\gamma'}\text{quarkContract13}(\Gamma^{B,T}U\Gamma^B,S)^{c'a}_{\beta'\beta'}\\
&+(PD)^{aa'}_{\gamma'\alpha'}\text{quarkContract13}(U,\Gamma^B S\Gamma^{B,T})^{a'a}_{\gamma'\alpha'}\\
&+2(PU)^{aa'}_{\gamma'\alpha'}\text{quarkContract13}(\Gamma^{B,T}D\Gamma^{B,T},S)^{a'a}_{\alpha'\gamma'}\\
&+(PU)^{aa'}_{\gamma'\alpha'}\text{quarkContract13}(D,\Gamma^B S\Gamma^{B,T})^{a'a}_{\gamma'\alpha'}\\
&-(PU)^{ac'}_{\gamma'\gamma'}\text{quarkContract13}(\Gamma^{B,T}D\Gamma^B,S)^{c'a}_{\beta'\beta'}.
\end{aligned}
$$

Some signs are changed due to the anti-symmetry of the Levi-Civita tensor. This subroutine is used to calculate the two-point function of the Λ-baryon.

## 4.2 Λ Three-point correlator

The Λ two-point-Correlator is as mentioned before:

$$
\begin{aligned}
P_{\gamma'\gamma}\langle\Lambda_\gamma\overline{\Lambda}_{\gamma'}\rangle = P_{\gamma'\gamma}\Big(&\underbrace{\epsilon_{abc}\big(\langle 2s^a_\gamma u^b_\beta(C\gamma_5)_{\beta\alpha}d^c_\alpha\rangle + \langle d^a_\gamma u^b_\beta(C\gamma_5)_{\beta\alpha}s^c_\alpha\rangle - \langle u^a_\gamma d^b_\beta(C\gamma_5)_{\beta\alpha}s^c_\alpha\rangle\big)}_{\Lambda}\\
&\cdot\underbrace{\epsilon_{a'b'c'}\big(\langle 2\overline{u}^{a'}_{\alpha'}(C\gamma_5)_{\alpha'\beta'}\overline{d}^{b'}_{\beta'}\overline{s}^{c'}_{\gamma'}\rangle + \langle\overline{u}^{a'}_{\alpha'}(C\gamma_5)_{\alpha'\beta'}\overline{s}^{b'}_{\beta'}\overline{d}^{c'}_{\gamma'}\rangle - \langle\overline{d}^{a'}_{\alpha'}(C\gamma_5)_{\alpha'\beta'}\overline{s}^{b'}_{\beta'}\overline{u}^{c'}_{\gamma'}\big)\rangle}_{\overline{\Lambda}}\Big)
\end{aligned}
$$

Now we want to insert a local operator $I$ at a space-time point $m$, to be able to calculate interactions with different currents. Depending on the operator we can insert it on every quark line. The Λ baryon has 3 different flavors u, d and s, where in the simulation the isospin limit is used ($m_u = m_d \neq 0$). The contractions are calculated for the three cases in which the operator is put on the u-, d-, and s-line. For each insertion a disconnected contribution appears which we neglect ( see fig 16). For demonstration we will do the contraction on the strange quark line ( s-line). The remaining insertions can be found in the appendix (A.3). With the insertion $I^s(m) = \overline{s}(m)^d_\delta \Gamma^{de}_{\delta\epsilon} s(m)^e_\epsilon$ in the s-line we get the three-point-correlator:

$$
C_{3pt} = P_{\gamma'\gamma}\langle\Lambda(n)_\gamma I^s(m)\overline{\Lambda}(0)_{\gamma'}\rangle
$$

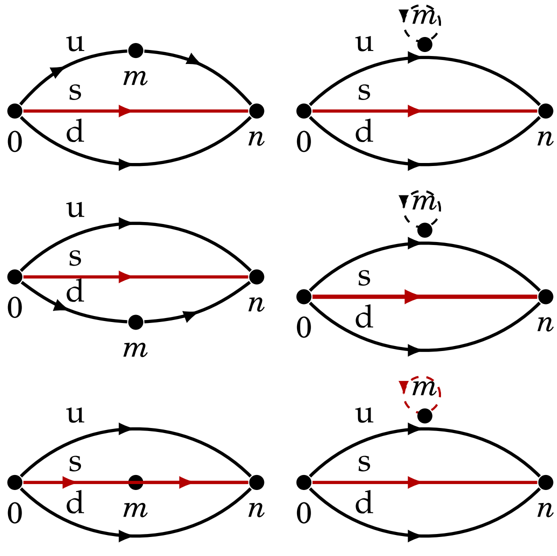


**Figure 16:** Insertion operator on the u-, d-, and s-line (from above). The dashed line indicates the disconnected contribution.

Inserting the explicit expression for the interpolator we get,

$$
\begin{aligned}
&P_{\gamma'\gamma}\langle \Lambda(n)_\gamma I(m)^s \overline{\Lambda}(0)_{\gamma'}\rangle = \\
&P^T_{\gamma\gamma'}\Big(\epsilon_{abc}\big(\langle 2s(n)^a_\gamma u(n)^b_\beta (C\gamma_5)_{\beta\alpha} d(n)^c_\alpha\rangle + \langle d(n)^a_\gamma u(n)^b_\beta (C\gamma_5)_{\beta\alpha} s(n)^c_\alpha\rangle - \\
&\langle u(n)^a_\gamma d(n)^b_\beta (C\gamma_5)_{\beta\alpha} s(n)^c_\alpha\rangle\big)\cdot \overline{s}(m)^d_\delta \Gamma^{de}_{\delta\epsilon} s(m)^e_\epsilon \cdot \epsilon_{a'b'c'}\big(\langle 2\overline{u}(0)^{a'}_{\alpha'} (C\gamma_5)_{\alpha'\beta'} \overline{d}(0)^{b'}_{\beta'} \overline{s}(0)^{c'}_{\gamma'}\rangle + \\
&\langle \overline{u}(0)^{a'}_{\alpha'} (C\gamma_5)_{\alpha'\beta'} \overline{s}(0)^{b'}_{\beta'} \overline{d}(0)^{c'}_{\gamma'}\rangle - \langle \overline{d}(0)^{a'}_{\alpha'} (C\gamma_5)_{\alpha'\beta'} \overline{s}(0)^{b'}_{\beta'} \overline{u}(0)^{c'}_{\gamma'})\rangle\Big)
\end{aligned}
$$

Now we factor out:

$$
\begin{aligned}
&P_{\gamma'\gamma}\langle \Lambda(n)_\gamma I(m)^s \overline{\Lambda}(0)_{\gamma'}\rangle = \\
&P^T_{\gamma\gamma'}\epsilon_{abc}\epsilon_{a'b'c'}\Big(\langle 4s(n)^a_\gamma u(n)^b_\beta (C\gamma_5)_{\beta\alpha} d(n)^c_\alpha \overline{u}(0)^{a'}_{\alpha'} (C\gamma_5)_{\alpha'\beta'} \overline{d}(0)^{b'}_{\beta'} \overline{s}(0)^{c'}_{\gamma'} \cdot \overline{s}(m)^d_\delta \Gamma^{de}_{\delta\epsilon} s(m)^e_\epsilon\rangle + \\
&\langle 2s(n)^a_\gamma u(n)^b_\beta (C\gamma_5)_{\beta\alpha} d(n)^c_\alpha \overline{u}(0)^{a'}_{\alpha'} (C\gamma_5)_{\alpha'\beta'} \overline{s}(0)^{b'}_{\beta'} \overline{d}(0)^{c'}_{\gamma'} \cdot \overline{s}(m)^d_\delta \Gamma^{de}_{\delta\epsilon} s(m)^e_\epsilon\rangle - \\
&\langle 2s(n)^a_\gamma u(n)^b_\beta (C\gamma_5)_{\beta\alpha} d(n)^c_\alpha \overline{d}(0)^{a'}_{\alpha'} (C\gamma_5)_{\alpha'\beta'} \overline{s}(0)^{b'}_{\beta'} \overline{u}(0)^{c'}_{\gamma'} \cdot \overline{s}(m)^d_\delta \Gamma^{de}_{\delta\epsilon} s(m)^e_\epsilon\rangle + \\
&\langle 2d(n)^a_\gamma u(n)^b_\beta (C\gamma_5)_{\beta\alpha} s(n)^c_\alpha \overline{u}(0)^{a'}_{\alpha'} (C\gamma_5)_{\alpha'\beta'} \overline{d}(0)^{b'}_{\beta'} \overline{s}(0)^{c'}_{\gamma'} \cdot \overline{s}(m)^d_\delta \Gamma^{de}_{\delta\epsilon} s(m)^e_\epsilon\rangle + \\
&\langle d(n)^a_\gamma u(n)^b_\beta (C\gamma_5)_{\beta\alpha} s(n)^c_\alpha \overline{u}(0)^{a'}_{\alpha'} (C\gamma_5)_{\alpha'\beta'} \overline{s}(0)^{b'}_{\beta'} \overline{d}(0)^{c'}_{\gamma'} \cdot \overline{s}(m)^d_\delta \Gamma^{de}_{\delta\epsilon} s(m)^e_\epsilon\rangle - \\
&\langle d(n)^a_\gamma u(n)^b_\beta (C\gamma_5)_{\beta\alpha} s(n)^c_\alpha \overline{d}(0)^{a'}_{\alpha'} (C\gamma_5)_{\alpha'\beta'} \overline{s}(0)^{b'}_{\beta'} \overline{u}(0)^{c'}_{\gamma'} \cdot \overline{s}(m)^d_\delta \Gamma^{de}_{\delta\epsilon} s(m)^e_\epsilon\rangle - \\
&\langle 2u(n)^a_\gamma d(n)^b_\beta (C\gamma_5)_{\beta\alpha} s(n)^c_\alpha \overline{u}(0)^{a'}_{\alpha'} (C\gamma_5)_{\alpha'\beta'} \overline{d}(0)^{b'}_{\beta'} \overline{s}(0)^{c'}_{\gamma'} \cdot \overline{s}(m)^d_\delta \Gamma^{de}_{\delta\epsilon} s(m)^e_\epsilon\rangle - \\
&\langle u(n)^a_\gamma d(n)^b_\beta (C\gamma_5)_{\beta\alpha} s(n)^c_\alpha \overline{u}(0)^{a'}_{\alpha'} (C\gamma_5)_{\alpha'\beta'} \overline{s}(0)^{b'}_{\beta'} \overline{d}(0)^{c'}_{\gamma'} \cdot \overline{s}(m)^d_\delta \Gamma^{de}_{\delta\epsilon} s(m)^e_\epsilon\rangle + \\
&\langle u(n)^a_\gamma d(n)^b_\beta (C\gamma_5)_{\beta\alpha} s(n)^c_\alpha \overline{d}(0)^{a'}_{\alpha'} (C\gamma_5)_{\alpha'\beta'} \overline{s}(0)^{b'}_{\beta'} \overline{u}(0)^{c'}_{\gamma'} \cdot \overline{s}(m)^d_\delta \Gamma^{de}_{\delta\epsilon} s(m)^e_\epsilon\rangle\Big)
\end{aligned}
$$

With the contraction $\langle f^a_\alpha \overline{f}^b_\beta \rangle = F^{ab}_{\alpha\beta}$ we get

$$P\gamma'\gamma \langle \Lambda(n)_\gamma I(m)^s \overline{\Lambda}(0)_{\gamma'} \rangle = P^T_{\gamma\gamma'} \epsilon_{abc}\epsilon_{a'b'c'} \Gamma^{de}_{\delta\epsilon} \overbrace{(C\gamma_5)_{\beta\alpha}}^{(\Gamma^B)_{\beta\alpha}} \overbrace{(C\gamma_5)_{\alpha'\beta'}}^{(\tilde{\Gamma}^B)_{\alpha'\beta'}}$$
$$\big(-4S(n,m)^{ad}_{\gamma\delta} S(m,0)^{ec'}_{\epsilon\gamma'} D(n,0)^{cb'}_{\alpha\beta'} U(n,0)^{ba'}_{\beta\alpha'} + 2U(n,0)^{ba'}_{\beta\alpha'} S(n,m)^{ad}_{\gamma\delta} D(n,0)^{cc'}_{\alpha\gamma'} S(m,0)^{eb'}_{\epsilon\beta'} +$$
$$2U(n,0)^{bc'}_{\beta\gamma'} S(n,m)^{ad}_{\gamma\delta} D(n,0)^{ca'}_{\alpha\alpha'} S(m,0)^{eb'}_{\epsilon\beta'} + 2D(n,0)^{ab'}_{\gamma\beta'} S(n,m)^{cd}_{\alpha\delta} U(n,0)^{ba'}_{\beta\alpha'} S(m,0)^{ec'}_{\epsilon\gamma'} -$$
$$D(n,0)^{ac'}_{\gamma\gamma'} S(n,m)^{cd}_{\alpha\delta} U(n,0)^{ba'}_{\beta\alpha'} S(m,0)^{eb'}_{\epsilon\beta'} - D(n,0)^{aa'}_{\gamma\alpha'} S(n,m)^{cd}_{\alpha\delta} U(n,0)^{bc'}_{\beta\gamma'} S(m,0)^{eb'}_{\epsilon\beta'} +$$
$$2S(n,m)^{cd}_{\alpha\delta} D(n,0)^{bb'}_{\beta\beta'} U(n,0)^{bb'}_{\beta\beta'} S(m,0)^{ec'}_{\epsilon\gamma'} - S(n,m)^{cd}_{\alpha\delta} D(n,0)^{bc'}_{\beta\gamma'} U(n,0)^{bc'}_{\beta\gamma'} S(m,0)^{eb'}_{\epsilon\beta'} -$$
$$S(n,m)^{cd}_{\alpha\delta} D(n,0)^{ba'}_{\beta\alpha'} U(n,0)^{ba'}_{\beta\alpha'} S(m,0)^{eb'}_{\epsilon\beta'}\big).$$

In our case $\Gamma^B$=$\tilde{\Gamma}^B$. The contractions lead us to the propagator $S(n,m)$, which is the propagator from the insertion point $m$ to the sink $n$. This propagator requires a calculation of an all-to-all propagator, as only the source at 0 is fixed. To avoid this computational task, we introduce the so-called *extended propagator* $\Sigma$. The three-point-correlator can be calculated with this extended propagator via

$$C_{3pt,s} = \Sigma(0,m)^{zd}_{\tau\delta} \Big(IS(m,0)\Big)^{dz}_{\delta\tau}. \tag{142}$$

To extract the $\Sigma$ we have first to factoring out $S(m,0)^{ec'}_{\epsilon\gamma'}$ and $S(m,0)^{eb'}_{\epsilon\beta'}$:

$$P_{\gamma'\gamma} \langle \Lambda(n)_\gamma I(m)^s \overline{\Lambda}(0)_{\gamma'} \rangle = P^T_{\gamma\gamma'} \epsilon_{abc}\epsilon_{a'b'c'} \Gamma^{de}_{\delta\epsilon} (\Gamma^B)_{\beta\alpha} (\tilde{\Gamma}^B)_{\alpha'\beta'}$$
$$\Big(S(m,0)^{ec'}_{\epsilon\gamma'} \Big(-4S(n,m)^{ad}_{\gamma\delta} U(n,0)^{ba'}_{\beta\alpha'} D(n,0)^{cb'}_{\alpha\beta'} + 2U(n,0)^{ba'}_{\beta\alpha'} D(n,0)^{ab'}_{\gamma\beta'} S(n,m)^{cd}_{\alpha\delta} +$$
$$2D(n,0)^{bb'}_{\beta\beta'} U(n,0)^{aa'}_{\gamma\alpha'} S(n,m)^{cd}_{\alpha\delta}) +$$
$$S(m,0)^{eb'}_{\epsilon\beta'} (2D(n,0)^{cc'}_{\alpha\gamma'} U(n,0)^{ba'}_{\beta\alpha'} S(n,m)^{ad}_{\gamma\delta} + 2D(n,0)^{ca'}_{\alpha\alpha'} U(n,0)^{bc'}_{\beta\gamma'} S(n,m)^{ad}_{\gamma\delta} -$$
$$U(n,0)^{ba'}_{\beta\alpha'} D(n,0)^{ac'}_{\gamma\gamma'} S(n,m)^{cd}_{\alpha\delta} - U(n,0)^{bc'}_{\beta\gamma'} D(n,0)^{aa'}_{\gamma\alpha'} S(n,m)^{cd}_{\alpha\delta}$$
$$-U(n,0)^{aa'}_{\gamma\alpha'} D(n,0)^{bc'}_{\beta\gamma'} S(n,m)^{cd}_{\alpha\delta} - U(n,0)^{ac'}_{\gamma\gamma'} D(n,0)^{ba'}_{\beta\alpha'} S(n,m)^{cd}_{\alpha\delta}\Big)\Big)$$

For $\Sigma$ we then get (consider the change of the indices: $c' \longrightarrow z$, $\gamma' \longrightarrow \tau$ for the first

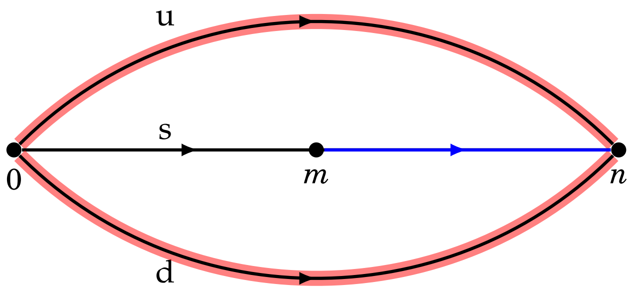


**Figure 17:** Fixed sink method: The source $\eta$ is colored red, whereas the extended propagator $\Sigma$ is blue, consider that also the source belongs to the extended propagator.

and $b' \longrightarrow z, \beta' \longrightarrow \tau$ for the second bracket )

$$
\begin{aligned}
&\Sigma(0,m)^{zd}_{\tau\delta} = \epsilon_{abc}(\Gamma^B)_{\beta\alpha} \\
&\Big(P^T_{\gamma\tau}\epsilon_{a'b'z}(\tilde{\Gamma}^B)_{\alpha'\beta'}\Big(-4D(n,0)^{cb'}_{\alpha\beta'}U(n,0)^{ba'}_{\beta\alpha'}S(n,m)^{ad}_{\gamma\delta} + 2D(n,0)^{ab'}_{\gamma\beta'}U(n,0)^{ba'}_{\beta\alpha'}S(n,m)^{cd}_{\alpha\delta} \\
&+ 2U(n,0)^{aa'}_{\gamma\alpha'}S(n,m)^{cd}_{\alpha\delta}D(n,0)^{bb'}_{\beta\beta'}\Big) \\
&P^T_{\gamma\gamma'}\epsilon_{a'zc'}(\tilde{\Gamma}^B)_{\alpha'\tau}\Big(2U(n,0)^{ba'}_{\beta\alpha'}S(n,m)^{ad}_{\gamma\delta}D(n,0)^{cc'}_{\alpha\gamma'} + 2U(n,0)^{bc'}_{\beta\gamma'}S(n,m)^{ad}_{\gamma\delta}D(n,0)^{ca'}_{\alpha\alpha'} - \\
&D(n,0)^{ac'}_{\gamma\gamma'}U(m,0)^{ba'}_{\beta\alpha'}S(n,m)^{cd}_{\alpha\delta} - D(n,0)^{aa'}_{\gamma\alpha'}U(n,0)^{bc'}_{\beta\gamma'}S(n,m)^{cd}_{\alpha\delta} - \\
&D(n,0)^{bc'}_{\beta\gamma'}U(n,0)^{aa'}_{\gamma\alpha'}S(n,m)^{cd}_{\alpha\delta} - D(n,0)^{ba'}_{\beta\alpha'}U(n,0)^{ac'}_{\gamma\gamma'}S(n,m)^{cd}_{\alpha\delta}\Big)\Big).
\end{aligned}
$$

The extended propagator can be computed with same procedure as the normal propagators $D$ and $U$. By introducing a sink $\eta$ we get

$$
\sum_m \Sigma(0,m)^{zd}_{\tau\delta}A(m,z)^{df}_{\delta\sigma} = \eta(0,z)^{zf}_{\tau\sigma}, \tag{143}
$$

where $A$[1] is the Dirac operator. This method is known as the fixed sink method [35] and is shown in figure 17. With

$$
(A^{-1})^{fd}_{\sigma\delta} = \begin{cases} S(n,m)^{ad}_{\gamma\delta}, & a \longrightarrow f, \gamma \longrightarrow \sigma, \\ S(n,m)^{cd}_{\alpha\delta}, & c \longrightarrow f, \alpha \longrightarrow \sigma, \end{cases}
$$

[1] In this case we have to choose this notation to distinguish the Dirac operator from the propagator of the d-quark

we get for the s-type source

$$\eta(0,z)^{zf}_{\tau\sigma} = \epsilon_{fbc}(\Gamma^B)_{\beta\alpha}$$
$$\Big(P^T_{\sigma\tau}\epsilon_{a'b'z}(\tilde{\Gamma}^B)_{\alpha'\beta'}\Big(-4U(z,0)^{ba'}_{\beta\alpha'}D(z,0)^{cb'}_{\alpha\beta'}\Big)+\Gamma^T_{\sigma\gamma'}\epsilon_{a'zc'}(\tilde{\Gamma}^B)_{\alpha'\tau}\Big(2U(z,0)^{ba'}_{\beta\alpha'}D(z,0)^{cc'}_{\alpha\gamma'}+$$
$$2D(z,0)^{ca'}_{\alpha\alpha'}U(z,0)^{aa'}_{\gamma\alpha'}\Big)\Big)+$$
$$\epsilon_{abf}(\Gamma^B)_{\beta\sigma}\Big(P^T_{\gamma\tau}\epsilon_{a'b'z}(\tilde{\Gamma^B})_{\alpha'\beta'}\Big(2D(z,0)^{ab'}_{\gamma\beta'}U(z,0)^{ba'}_{\beta\alpha'}+2D(z,0)^{bb'}_{\beta\beta'}U(z,0)^{aa'}_{\gamma\alpha'}\Big)+$$
$$P^T_{\gamma\gamma'}\epsilon_{a'zc'}(\tilde{\Gamma}^B)_{\alpha'\tau}\Big(-D(z,0)^{ac'}_{\gamma\gamma'}U(z,0)^{ba'}_{\beta\alpha'}-D(z,0)^{aa'}_{\gamma\alpha'}U(z,0)^{bc'}_{\beta\gamma'}-U(z,0)^{aa'}_{\gamma\alpha'}D(z,0)^{bc'}_{\beta\gamma'}-$$
$$D(z,0)^{ba'}_{\beta\alpha'}U(z,0)^{ac'}_{\gamma\gamma'}\Big)\Big).$$

In the final step, we get the QDP-code

$$\begin{aligned}= \text{-4quarkContract24}(&(\Gamma^B)^T U, D(\tilde{\Gamma}^B)^T)^{zf}_{\alpha\alpha}P_{\tau\sigma} - 2\text{quarkContract13}(\Gamma^B DP, U\tilde{\Gamma}^B)^{zf}_{\sigma\tau}+\\
&2\text{quarkContract13}(\Gamma^B D\tilde{\Gamma}^B, UP)^{zf}_{\tau\sigma} - 2\text{quarkContract24}(PD(\tilde{\Gamma}^B)^T, (\Gamma^B)^T U)^{zf}_{\tau\sigma}+\\
&2\text{quarkContract24}(PU\tilde{\Gamma}^B, (\Gamma^B)^T D)^{zf}_{\tau\sigma} - \text{quarkContract34}((\Gamma^B)^T U\tilde{\Gamma}^B, PD)^{zf}_{\sigma\tau}+\\
&\text{quarkContract14}(PD\tilde{\Gamma}^B, (\Gamma^B)^T U)^{zf}_{\tau\sigma} + \text{quarkContract14}(PU\tilde{\Gamma}^B, (\Gamma^B)^T D)^{zf}_{\tau\sigma}-\\
&\text{quarkContract34}((\Gamma^B)^T D\tilde{\Gamma}^B, PU)^{zf}_{\sigma\tau}.\end{aligned}$$

Signs changed due to the anti-symmetry of the Levi-Civita Tensor.

## 4.3 Results

The axial current is not conserved due to the breaking of chiral symmetry (see eq. (56)). The renormalization of the axial current in O(a) improved lattice QCD is done with the defintion [55]

$$(A^i_R)_\mu(n) = Z_A\left(1+b_A a m_q\right)(A^i_\mu(n) + \underbrace{a c_A \partial_\mu P^i(n)}_{\text{improvement Term}}). \tag{144}$$

The quark mass is denoted by $m_q$ and $P(n)$ is the pseudo-scalar density, defined as

$$P^i(n) = \overline{\psi}(n)\gamma_5\frac{\lambda^i}{2}\psi(n). \tag{145}$$

The derivative of $P(n)$ vanishes for zero momentum. Since the axial charge is calculated using zero momentum, we can omit the improvement term. The renormalization factor $Z_A$ has been determined in [55] to $Z_A = 0.724$. The mass-dependent term proportional to the coefficient $b_A$, which is determined in [56], will be dropped. The exact value of the term don't exists for this thesis, but first estimations leads

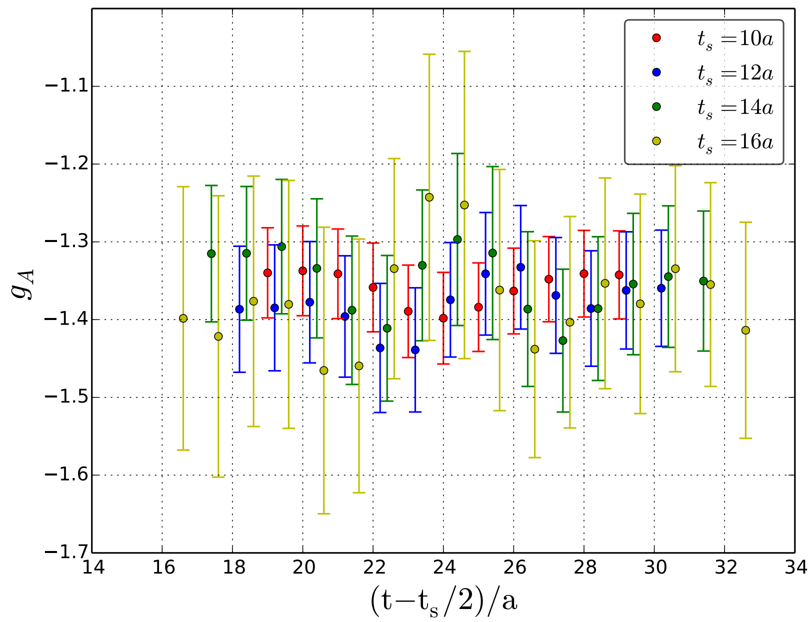


**Figure 18:** $g_A$ on H105 at different source-sink separation $t_s$, averaged over 600 measurements.

to a contribution of ~ 3% with $\kappa_c \sim 0.137142$. In figure 18 we see the values of $g_A$ . They are calculated for four different source-sink separations $t_s$ (10 a, 12 a, 14 a and 16 a) on the H105 ensemble over 600 configurations. We used smeared-smeared propagators for the two- and three-point correlators. The values are displaced by $\frac{t_s}{2}$ for better visibility. To distinguish the single points, the values of each source-sink separation are shifted by 0.2 a. Excited states are suppressed for large $t$, however a large $t$ causes an increase in noise, which makes a larger source-sink separations impossible. We assume, that the correlator is slightly contaminated by excited states, as the plot in 18 does not differ strongly in $t_s$. To extract $g_A$ we fit a constant to the ratio

$$f(t) = g_A,$$

which we refer to as *plateau method*. Figure 19 shows the constant fits to different source-sink separations. We will take the value at $t_s = 10\,\mathrm{a}$ due to the small error,

$$g_A^{\text{cons.fit}} = -1.36 \pm 0.06. \tag{146}$$

### 4.3.1 Summation method

We want to examine, if $g_A$ is strongly contaminated by excited states. To check for contamination from excited states we use the summation method [44]. We

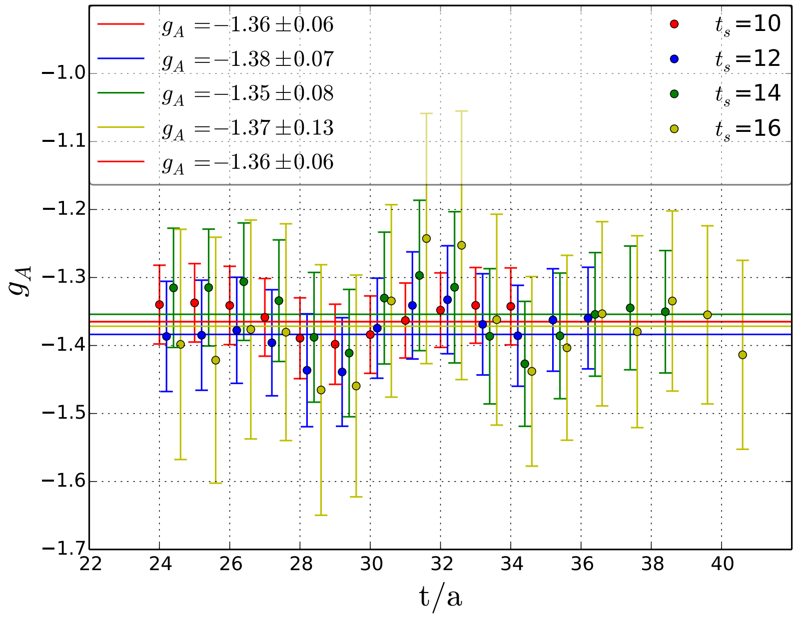


**Figure 19:** Constant fit to all source-sink separation on H105.

consider excited states by using the ratio

$$R_{A_3} = R_{A_3}^{\text{ground}}\left(1 + \mathcal{O}(e^{\Delta t}) + \mathcal{O}(e^{-\Delta(t_s - t)}) + \mathcal{O}(e^{\Delta t_s})\right), \tag{147}$$

where $R_{A_3}^{\text{ground}}$ is the ratio only considering the ground state and $\Delta = m_{\text{excited}} - m_\Lambda$ the energy gap between ground and excited state. If we sum the ratio over the whole range of insertion time we get [45]

$$R_{A_3}^{\text{sum}} = \sum_{t=0}^{t_s} R_{A_3} \longrightarrow c + t_s\left(g_A^{\text{bare}} + \mathcal{O}\left(e^{-\Delta t_s}\right)\right). \tag{148}$$

where $g_A^{\text{bare}}$ is the unrenormalized value of $g_A$. We see that the excited-state contributions are reduced, since $t_s$ >($t_s$ - $t$ ). Performing this summation for several $t_s$, we can extract $g_A$ from the slope of a linear fit,

$$f(t_s) = g_A t_s + c. \tag{149}$$

Figure 20 shows the linear fit to the four source-sink separations. Measuring the slope, we get for renormalized $g_A$

$$g_A^{\text{sum}} = -1.38 \pm 0.30. \tag{150}$$

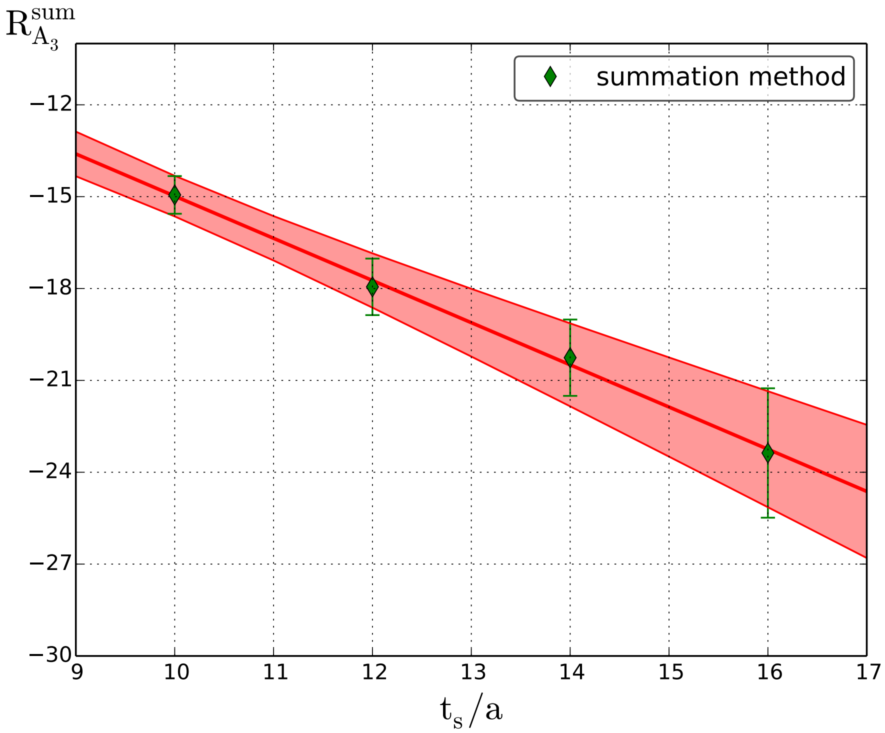


**Figure 20:** $g_A$ extracted from slope of the linear fit over four source-sink separation

Here again the error grows with larger $t_s$. The error of $g_A^{sum}$ was also calculated with the Jackknife method. Comparing eq. (146) and eq. (150) we see that the values are entirely consistent, which confirms our statement of the low contamination by excited states. In the next chapter we will extrapolate the values to the physical masses, for that we have to do the lattice calculation on multiple ensembles.

# 5 Results at the physical point

In this section we want to extrapolate our results $m_\Lambda$ and $g_A$ to the physical pion and kaon masses. To extrapolate to the physical masses we add to the results of the H105 ensemble the calculations on the H102 and C101 ensembles at different pion and kaon masses. The fit functions are derived from SU(3) chiral perturbation theory ($\chi$PT).

## 5.1 Physical point: Mass

The extrapolation formula from SU(3) $\chi$PT for thr octet baryon mass in terms of kaon and pion masses to order $\mathcal{O}(p^2)$ are given by [58, 59]

$$\begin{aligned} M_N &= m_0 - 4b_D\dot{M}_K^2 + 4b_F\left(\dot{M}_K^2 - \dot{M}_\pi^2\right) - 2b_0\left(2\dot{M}_K^2 + \dot{M}_\pi^2\right) + \mathcal{O}(p^2), \\ M_\Lambda &= m_o + \frac{4}{3}b_D\left(-4\dot{M}_K^2 + \dot{M}_\pi^2\right) - 2b_0\left(2\dot{M}_K^2 + \dot{M}_\pi^2\right) + \mathcal{O}(p^2), \\ M_\Sigma &= m_0 - 4b_D\dot{M}_\pi^2 - 2b_0\left(2\dot{M}_K^2 + \dot{M}_\pi^2\right) + \mathcal{O}(p^2), \\ M_\Xi &= m_0 - 4b_D\dot{M}_K^2 - 4b_F\left(\dot{M}_K^2 - \dot{M}_\pi^2\right) - 2b_0\left(2\dot{M}_K^2 + \dot{M}_\pi^2\right) + \mathcal{O}(p^2), \end{aligned} \tag{151}$$

with $m_0$ the average octet mass in the chiral limit. The dot denotes the leading order in the quark mass expansion [61]. In this thesis we work in the isospin limit, which implies setting the light quark masses $m_l$ to

$$m_l = m_u = m_d,$$

with $m_u$ the up-quark mass and $m_d$ the down-quark mass. There are some combinations of hadron masses which are stable when $m_l$ and $m_s$ is varied while the average quark mass is fixed $\overline{m} = \frac{1}{3}(2m_l + m_s)$ [61]. Fixing the mass has the advantage, that one gets a linear behavior of $\nu \sim \frac{M_K^2 + M_\pi^2}{2}$ to a mass ratio $f_B$ (explanation below). On our ensembles this strategy is equivalent to keep the bare quark mass fixed [62]

$$C = \sum_{f=1}^{3} \frac{1}{\kappa_f} = \text{const.}, \tag{152}$$

which has the value of $C \approx 10.96815$ for the three ensembles H102, H105 and C101. One of the stable combinations mentioned before is the average nucleon-mass which is defined as [60]

$$X_N^{\text{phys}} = \frac{1}{3}(M_N + M_\Sigma + M_\Xi) \approx 1149\,\text{MeV}. \tag{153}$$

It is evaluted at the physical masses $M_N \approx 940\,\text{MeV}$, $M_\Sigma \approx 1192\,\text{MeV}$ and $M_\Xi \approx 1314\,\text{MeV}$ (PDG). Inserting the mass from eq. (151) we get

$$X_N = m_0 - 2b_0\left(2M_K^2 + M_\pi^2\right) + \dots . \tag{154}$$

It can be shown that the ratio

$$f_B = \frac{M_B}{X_N} \qquad \text{for} \quad B = N, \Lambda, \Sigma, \Xi \tag{155}$$

is linear in the dimensionless quantity $\nu = \frac{M_\pi^2 - X_\pi^2}{X_\pi^2}$ [61] at first order of the double expansion, the chiral expansion plus the expansion in $\delta m_l = m_l - \overline{m}$. The stable average pion mass is defined as

$$X_\pi = \frac{1}{3}\left(2M_K^2 + M_\pi^2\right).$$

The value of $\nu$ at physical pion and kaon mass is

$$\nu^{\text{phys}} = -0.89.$$

For the leading order contribution the kaon mass $\dot{M}_K^2$ and pion mass $\dot{M}_\pi^2$ are

$$\dot{M}_\pi^2 = 2B_0\overline{m} + 2B_0\delta m_l,$$
$$\dot{M}_K^2 = 2B_0\overline{m} - 2B_0\delta m_l,$$

which shows that $\nu$ parametrizes SU(3) symmetry breaking (for $m_s = m_l = \overline{m} \longrightarrow \nu = 0$). The ratio can approximately be written as

$$f_B(\nu) \approx 1 + c\nu.$$

Motivated by this we choose the fit function

$$f(\nu) = 1 + b\nu.$$

We will fit the ratio $\frac{M_\Lambda}{X_N}$ with the $\Lambda$-mass $M_\Lambda$ calculated on the H105, H102 and C101 ensemble (see appendix A.4). We get

$$\frac{M_\Lambda}{X_N}\left(\nu^{\text{phys}}\right) \approx (0.94 \pm 0.02). \tag{156}$$

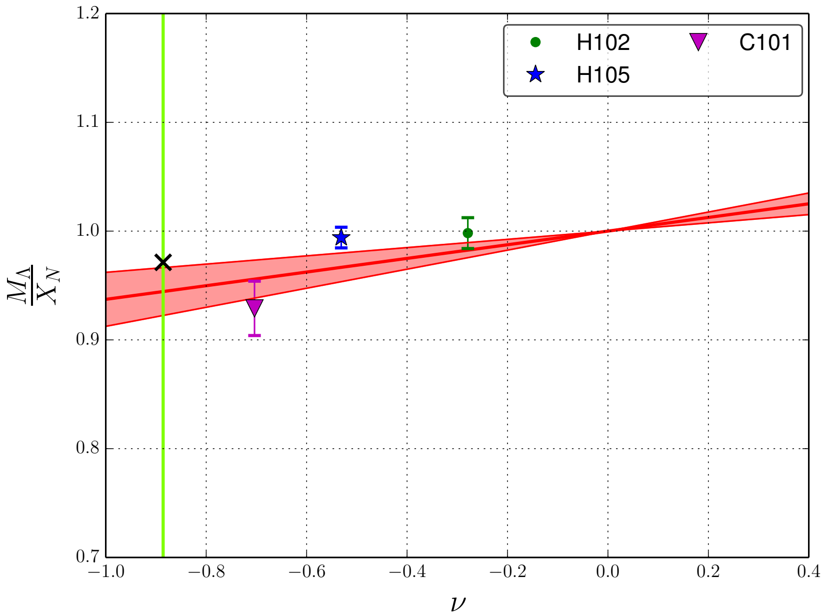


**Figure 21:** Chiral behaviour of the mass ratio $\frac{M_\Lambda}{X_N}$. The vertical line indicates the physical area $\nu^{\text{phys}}$, where $\frac{M_\lambda^{\text{phys}}}{X_N}$ is depicted by the black cross

This is the result at physical pion and kaon masses. The C101 value dominates the fit. The larger error of C101 and H102 arises from the low statistics, 139 measurements for C101 and 150 for H102. Better results can be achieved by increasing statistics, especially for C101 and H102. From eq. (156) we can calculate the Λ-mass $M_\lambda^l$ , we get

$$M_\lambda^l = 1085 \pm 25\text{MeV}$$

The value did not agree with the physical mass of $M_\Lambda^{\text{phys}} = 1117$ [MeV] ( see [30] ). There is still room for improvement : Firstly, we did not extrapolate to the continuum limit, since the computational effort required to compute the desired observable on multiple ensembles with different lattice spacing was beyond the scope of this thesis. Secondly, we performed the calculations on 2+1 ensembles, whereas in nature $N_f$=1+1+1+1[1] holds. Thirdly, more ensembles would improve the description of the chiral behavior.

## 5.2 Physical point: Axial charge

Here we extrapolate the axial charge to the physical point with the ansatz given in [63]. The ratio of three and two point functions in eq.(110) can be linearized in

[1]The bottom and top quarks are too heavy

terms of $(M_K^2 + M_\pi^2)$ and so its valid for $g_A$, as it can be extracted from the ratio,

$$g_A = a + b\left(M_K^2 + M_\pi^2\right). \tag{157}$$

We do an extrapolation for both of the values obtained from the summation and the plateau method. Since we average only over 138 measurements on C101 and 150 on H102, we see a big statistical error on both values (figure 22). The intercept with the physical mass line of the plateau and summation fit is

$$g_{\text{A,Plateau}} = -1.35 \pm 0.13 \tag{158}$$

$$g_{\text{A,Summation}} = -1.24 \pm 0.68 \tag{159}$$

The axial charge extracted from the summation method shows a larger error than the value extracted from the plateau method. An extrapolation to the continuum limit and larger statistics would improve the result. The axial charge, estimated from SU(3) symmetry don't lie in the error frame of $g_{\text{A,Plateau}}$. The deviation does not seems to be implausible, since we performing calculation on $N_f$=2+1 ensembles and have omitted the quark-disconnected parts. Nevertheless, as an orientation it shows us that the lattice calculation is capable of determining the axial charge of the $\Lambda$ baryon.

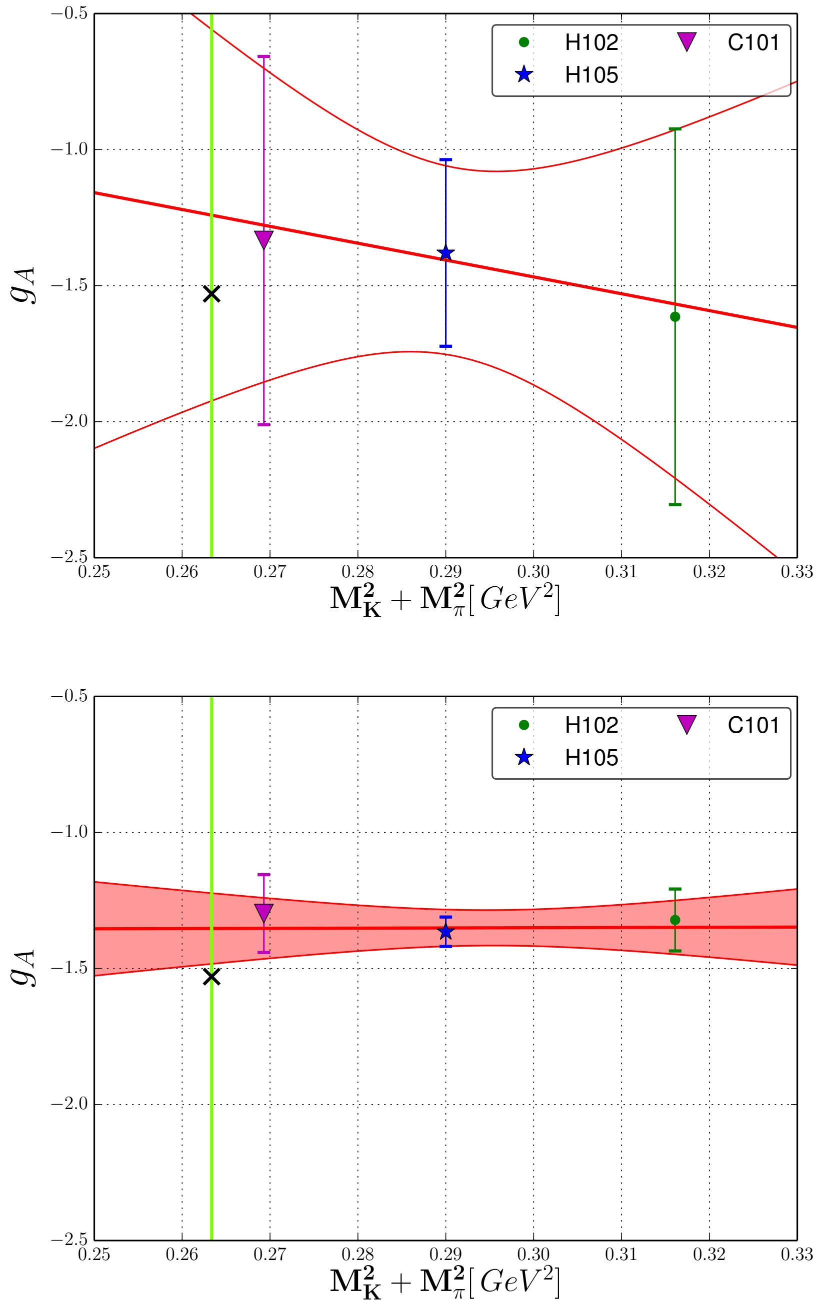


**Figure 22:** Chiral behaviour of $g_A$, extracted of the summation method (above) and the plateau method (below). The physical value (black cross) was estimated in section 2.7.

# 6 Summary and outlook

In this thesis, we provided a step by step analysis to calculate the Λ-baryon mass and the axial charge of the Λ in lattice QCD. The simulations are performed on an $N_f$=2+1 lattice with $\mathcal{O}$(a)-improved Wilson fermions and open boundary conditions. We calculated the 2- and 3-point function of the Λ-baryon on three ensemble H102, H105 and C101 with unphysical pion and kaon mass, ranging from $m_\pi$=220-350 MeV and $m_K$=440-470 MeV at a lattice spacing $a$ ≈0.086 fm.

By employing the 2-point correlation function we could obtain an *effective mass plateau*, that indicates the low lying energy states. With a constant fit, we extracted the mass as reasoned in section 3.2. We confirmed the signal-to-noise behavior, that the noise grows proportional to the exponential in lattice time direction, of the Λ-baryon on the H105 ensemble. In order to extrapolate the mass to the value with physical pion and kaon mass we constructed the ratio $\frac{M_\Lambda}{X_N}$. We calculated a Λ mass of 1141±7 MeV . This can be improved by adding more values on different ensembles to the extrapolation. Ensembles with different lattice spacings would make extrapolations to the continuum limit possible.

We derived the theoretical value of the isoscalar axialvector charge in flavor SU(3) with the Cabbibo scheme and used two methods, the plateau and summation method to extract the axial charge from the lattice calculations. The axial charge determined from the summation method did not differ much from the value determined from the plateau fits. Hence excited contributions seems to be negligible. We also extrapolate the axial charges to values with physical pion and kaon masses. Due to little measurements we get a big error for axial charge obtained from the summation method. The results can further be pushed to the physical value by extrapolating to the continuum limit. All measurements were done at four source positions, where in this thesis we used only one at $(0, 0, 0, 24)$. Measurements on different source positions would help to increase the statistic without requiring new configurations. The determination of the axial form factor of Λ remains. The correlation functions are already done for different momenta, hence the necessary data are already available.

# A Appendices

## A.1 Gamma matrices

The following Dirac matrices in Euclidean space are used in this thesis

$$\gamma_j^E = \begin{pmatrix} 0 & -i\sigma_j \\ i\sigma_j & 0 \end{pmatrix}, \qquad \gamma_0^E = \begin{pmatrix} 0 & 1 \\ 1 & 0 \end{pmatrix}, \qquad \gamma_5^E = \gamma_0^E\gamma_1^E\gamma_2^E\gamma_3^E = \begin{pmatrix} -1 & 0 \\ 0 & 1 \end{pmatrix}, \tag{160}$$

with the Pauli matrices

$$\sigma_1 = \begin{pmatrix} 0 & 1 \\ 1 & 0 \end{pmatrix}, \qquad \sigma_2 = \begin{pmatrix} 0 & -i \\ i & 0 \end{pmatrix}, \qquad \sigma_3 = \begin{pmatrix} 1 & 0 \\ 0 & -1 \end{pmatrix}. \tag{161}$$

The relations of the Dirac matrices in Euclidean and Minkowski space are

$$\gamma_0^E = \gamma_0^M, \qquad \gamma_5^E = \gamma_5^M, \qquad \gamma_i^E = -i\gamma_i^M. \tag{162}$$

## A.2 Gell-Mann matrices

A concrete representation is given by

$$\lambda_1 = \begin{pmatrix} 0 & 1 & 0 \\ 1 & 0 & 0 \\ 0 & 0 & 0 \end{pmatrix}, \qquad \lambda_2 = \begin{pmatrix} 0 & -i & 0 \\ i & 0 & 0 \\ 0 & 0 & 0 \end{pmatrix}, \qquad \lambda_3 = \begin{pmatrix} 1 & 0 & 0 \\ 0 & -1 & 0 \\ 0 & 0 & 0 \end{pmatrix}, \qquad \lambda_4 = \begin{pmatrix} 0 & 0 & 1 \\ 0 & 0 & 0 \\ 1 & 0 & 0 \end{pmatrix}$$

$$\lambda_5 = \begin{pmatrix} 0 & 0 & -i \\ 0 & 0 & 0 \\ i & 0 & 0 \end{pmatrix}, \qquad \lambda_6 = \begin{pmatrix} 0 & 0 & 0 \\ 0 & 0 & 1 \\ 0 & 1 & 0 \end{pmatrix}, \qquad \lambda_7 = \begin{pmatrix} 0 & 0 & 0 \\ 0 & 0 & -i \\ 0 & i & 0 \end{pmatrix}, \qquad \lambda_8 = \begin{pmatrix} 1 & 0 & 0 \\ 0 & 1 & 0 \\ 0 & 0 & -2 \end{pmatrix}.$$

## A.3 Three-point contraction for u- and d-insertion

### A.3.1 U-insertion

$$\begin{aligned}
&P_{\gamma'\gamma}\,\langle \Lambda(n)_\gamma I(m)^u \overline{\Lambda}(0)_{\gamma'}\rangle \\
&= P^T_{\gamma\gamma'}\Big(\epsilon_{abc}\big(\langle 2s(n)^a_\gamma u(n)^b_\beta (C\gamma_5)_{\beta\alpha} d(n)^c_\alpha\rangle + \langle d(n)^a_\gamma u(n)^b_\beta (C\gamma_5)_{\beta\alpha} s(n)^c_\alpha\rangle - \\
&\langle u(n)^a_\gamma d(n)^b_\beta (C\gamma_5)_{\beta\alpha} s(n)^c_\alpha\rangle\big)\cdot \overline{u}(m)^d_\delta \Gamma^{de}_{\delta\epsilon} u(m)^e_\epsilon \cdot \epsilon_{a'b'c'}\big(\langle 2\overline{u}(0)^{a'}_{\alpha'}(C\gamma_5)_{\alpha'\beta'}\overline{d}(0)^{b'}_{\beta'}\overline{s}(0)^{c'}_{\gamma'}\rangle + \\
&\langle \overline{u}(0)^{a'}_{\alpha'}(C\gamma_5)_{\alpha'\beta'}\overline{s}(0)^{b'}_{\beta'}\overline{d}(0)^{c'}_{\gamma'}\rangle - \langle \overline{d}(0)^{a'}_{\alpha'}(C\gamma_5)_{\alpha'\beta'}\overline{s}(0)^{b'}_{\beta'}\overline{u}(0)^{c'}_{\gamma'}\rangle\big)\Big)
\end{aligned}$$

With the Contraction $\langle f^a_\alpha \overline{f}^b_\beta \rangle = F^{ab}_{\alpha\beta}$ we get:

$$P_{\gamma'\gamma} \langle \Lambda(n)_\gamma I(m)^u \overline{\Lambda}(0)_{\gamma'} \rangle = P^T_{\gamma\gamma'} \epsilon_{abc} \epsilon_{a'b'c'} \Gamma^{de}_{\delta\epsilon} (C\gamma_5)_{\beta\alpha} (C\gamma_5)_{\alpha'\beta'}$$
$$\big( -4S(n,0)^{ac'}_{\gamma\gamma'} U(n,m)^{bd}_{\beta\delta} D(n,0)^{cb'}_{\alpha\beta'} U(m,0)^{ea'}_{\epsilon\alpha'} + 2S(n,0)^{ab'}_{\gamma\beta'} U(n,m)^{bd}_{\beta\delta} D(n,0)^{cc'}_{\alpha\gamma'} U(m,0)^{ea'}_{\epsilon\alpha'} +$$
$$2S(n,0)^{ab'}_{\gamma\beta'} U(n,m)^{bd}_{\beta\delta} D(n,0)^{ca'}_{\alpha\alpha'} U(m,0)^{ec'}_{\epsilon\gamma'} + 2D(n,0)^{ab'}_{\gamma\beta'} U(n,m)^{bd}_{\beta\delta} S(n,0)^{cc'}_{\alpha\gamma'} U(m,0)^{ea'}_{\epsilon\alpha'} -$$
$$D(n,0)^{ac'}_{\gamma\gamma'} U(n,m)^{bd}_{\beta\delta} S(n,0)^{cb'}_{\alpha\beta'} U(m,0)^{ea'}_{\epsilon\alpha'} - D(n,0)^{aa'}_{\gamma\alpha'} U(n,m)^{bd}_{\beta\delta} S(n,0)^{cb'}_{\alpha\beta'} U(m,0)^{ec'}_{\epsilon\gamma'} +$$
$$2U(n,m)^{ad}_{\gamma\delta} D(n,0)^{bb'}_{\beta\beta'} S(m,0)^{cc'}_{\alpha\gamma'} U(m,0)^{ea'}_{\epsilon\alpha'} - U(n,m)^{ad}_{\gamma\delta} D(n,0)^{bc'}_{\beta\gamma'} S(n,0)^{cb'}_{\alpha\beta'} U(m,0)^{ea'}_{\epsilon\alpha'} -$$
$$U(n,m)^{ad}_{\gamma\delta} D(n,0)^{ba'}_{\beta\alpha'} S(n,0)^{cb'}_{\alpha\beta'} U(m,0)^{ec'}_{\epsilon\gamma'} \big).$$

The extended source is

$$\eta(0,z)^{zf}_{\tau\sigma} = -4\epsilon_{zb'c'}\epsilon_{afc} S(z,0)^{ac'}_{\gamma\gamma'} P_{\gamma'\gamma} \Gamma^B_{\sigma\alpha} D(z,0)^{cb'}_{\alpha\beta'} \tilde{\Gamma}^{B^T}_{\beta'\tau} +$$
$$2\epsilon_{zb'c'}\epsilon_{afc} P_{\gamma'\gamma} S(z,0)^{ab'}_{\gamma\beta'} \tilde{\Gamma}^{B^T}_{\beta'\tau} \Gamma^B_{\sigma\alpha} D(z,0)^{cc'}_{\alpha\gamma'} +$$
$$2\epsilon_{zb'c'}\epsilon_{afc} P_{\gamma'\gamma} D(z,0)^{ab'}_{\gamma\beta'} \tilde{\Gamma}^{B^T}_{\beta'\tau} \Gamma^B_{\sigma\alpha} S(z,0)^{cc'}_{\alpha\gamma'} - \epsilon_{zb'c'}\epsilon_{afc} P_{\gamma'\gamma} D(z,0)^{ac'}_{\gamma\gamma'} \Gamma^B_{\sigma\alpha} S(z,0)^{cb'}_{\alpha\beta'} \tilde{\Gamma}^{B^T}_{\beta'\tau} +$$
$$2\epsilon_{zb'c'}\epsilon_{fbc} D(z,0)^{bb'}_{\beta\beta'} \tilde{\Gamma}^{B^T}_{\beta'\tau} \Gamma^B_{\beta\alpha} S(z,0)^{cc'}_{\alpha\gamma'} P_{\gamma'\sigma} - \epsilon_{zb'c'}\epsilon_{fbc} D(z,0)^{bc'}_{\beta\gamma'} P_{\gamma'\sigma} \Gamma^B_{\beta\alpha} S(z,0)^{cb'}_{\alpha\beta'} \tilde{\Gamma}^{B^T}_{\beta'\tau} -$$
$$\epsilon_{a'b'z}\epsilon_{fbc} \Gamma^{B^T}_{\alpha\beta} D(z,0)^{ba'}_{\beta\alpha'} S(z,0)^{cb'}_{\alpha\beta'} \tilde{\Gamma}^{B^T}_{\beta'\alpha'} P^T_{\sigma\tau} - \epsilon_{a'b'z}\epsilon_{afc} P_{\tau\gamma} D(z,0)^{aa'}_{\gamma\alpha'} \tilde{\Gamma}^B_{\alpha'\beta'} \Gamma^B_{\sigma\alpha} S(z,0)^{cb'}_{\alpha\beta'} +$$
$$2\epsilon_{a'b'z}\epsilon_{afc} P_{\tau\gamma} S(z,0)^{ab'}_{\gamma\beta'} \Gamma^B_{\sigma\alpha} D(z,0)^{ca'}_{\alpha\alpha'} \tilde{\Gamma}^B_{\alpha'\beta'}$$

which reads when converted to QDP operators

$$= -4\text{quarkContract12}\left(SP, \Gamma^B D (\tilde{\Gamma}^B)^T\right)^{zf}_{\sigma\tau} - 2\text{quarkContract14}\left(PS(\tilde{\Gamma}^B)^T, \Gamma^B D\right)^{zf}_{\tau\sigma} -$$
$$2\text{quarkContract14}\left(PD(\tilde{\Gamma}^B)^T, \Gamma^B S\right)^{zf}_{\tau\sigma} - \text{quarkContract12}\left(PD, \Gamma^B S (\tilde{\Gamma}^B)^T\right)^{zf}_{\sigma\tau} +$$
$$2\text{quarkContract13}\left(D(\tilde{\Gamma}^B)^T, \Gamma^B SP\right)^{zf}_{\tau\sigma} + \text{quarkContract13}\left(DP, \Gamma^B S(\tilde{\Gamma}^B)^T\right)^{zf}_{\sigma\tau} -$$
$$\text{quarkContract13}\left((\Gamma^B)^T D, S(\tilde{\Gamma}^B)^T\right)^{zf}_{\alpha'\alpha'} P^T_{\sigma\tau} + \text{quarkContract24}\left(PD\tilde{\Gamma}^B, \Gamma^B S\right)^{zf}_{\tau\sigma} +$$
$$2\text{quarkContract24}\left(PS, \Gamma^B D \tilde{\Gamma}^B\right)^{zf}_{\tau\sigma}.$$

### A.3.2 D-insertion

$$P_{\gamma'\gamma}\langle\Lambda(n)_\gamma I(m)^d\overline{\Lambda}(0)_{\gamma'}\rangle =$$
$$P^T_{\gamma\gamma'}\Big(\epsilon_{abc}\big(\langle 2s(n)^a_\gamma u(n)^b_\beta(C\gamma_5)_{\beta\alpha}d(n)^c_\alpha\rangle + \langle d(n)^a_\gamma u(n)^b_\beta(C\gamma_5)_{\beta\alpha}s(n)^c_\alpha\rangle -$$
$$\langle u(n)^a_\gamma d(n)^b_\beta(C\gamma_5)_{\beta\alpha}s(n)^c_\alpha\rangle\big)\cdot\overline{d}(m)^d_\delta\Gamma^{de}_{\delta\epsilon}d(m)^e_\epsilon\cdot\epsilon_{a'b'c'}\big(\langle 2\overline{u}(0)^{a'}_{\alpha'}(C\gamma_5)_{\alpha'\beta'}\overline{d}(0)^{b'}_{\beta'}\overline{s}(0)^{c'}_{\gamma'}\rangle +$$
$$\langle\overline{u}(0)^{a'}_{\alpha'}(C\gamma_5)_{\alpha'\beta'}\overline{s}(0)^{b'}_{\beta'}\overline{d}(0)^{c'}_{\gamma'}\rangle - \langle\overline{d}(0)^{a'}_{\alpha'}(C\gamma_5)_{\alpha'\beta'}\overline{s}(0)^{b'}_{\beta'}\overline{u}(0)^{c'}_{\gamma'}\rangle\big)\Big).$$

The QDP operators for the extended source is

$$= \text{-4quarkContract12}\Big(PS,(\Gamma^B)^T U\tilde{\Gamma}^B\Big)^{zf}_{\sigma\tau} - \text{2quarkContract24}\Big(PS,(\Gamma^B)^T U\tilde{\Gamma}^B\Big)^{zf}_{\tau\sigma} +$$
$$\text{2quarkContract14}\Big(PS(\tilde{\Gamma}^B)^T,(\Gamma^B)^T U\Big)^{zf}_{\tau\sigma} - \text{2quarkContract13}\Big(SP,(\Gamma^B)^T U\tilde{\Gamma}^B\Big)^{zf}_{\sigma\tau} -$$
$$\text{quarkContract13}\Big(S(\tilde{\Gamma}^B)^T,(\Gamma^B)^T U\Big)^{zf}_{\alpha'\alpha'}P_{\tau\sigma} + \text{quarkContract13}\Big(S(\tilde{\Gamma}^B)^T,(\Gamma^B)^T UP\Big)^{zf}_{\tau\sigma} +$$
$$\text{2quarkContract23}\Big(\Gamma^B SP,U\tilde{\Gamma}^B\Big)^{zf}_{\sigma\tau} + \text{quarkContract24}\Big(\Gamma^B S(\tilde{\Gamma}^B)^T,PU\Big)^{zf}_{\sigma\tau} -$$
$$\text{quarkContract34}\Big(\Gamma^B S(\tilde{\Gamma}^B)^T,PU\Big)^{zf}_{\sigma\tau}.$$

## A.4 Effective mass plots

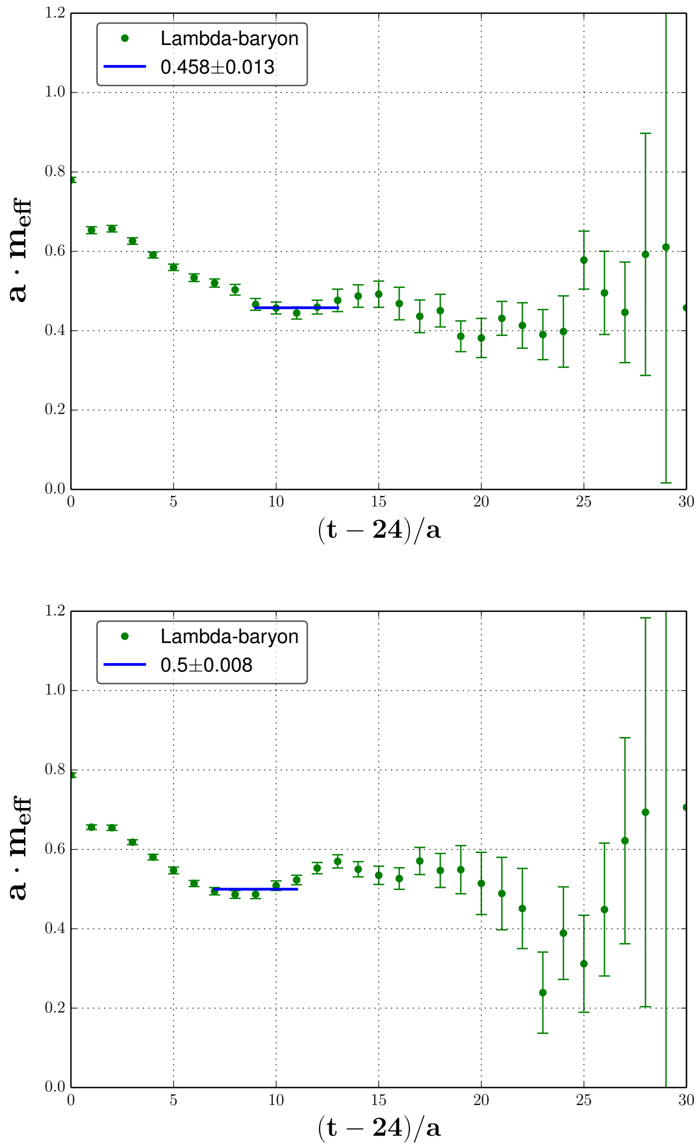


**Figure 23:** Smeared-point effective mass plot on the C101 (above) and H102 (below) ensemble with 139 and 150 measurments.

With the effective masses

$$M_\Lambda^{H102} = 1146 \pm 16\,\text{MeV}, \qquad M_\Lambda^{H105} = 1143 \pm 14\,\text{MeV}, \qquad M_\Lambda^{C101} = 1159 \pm 26\,\text{MeV}.$$

# References

[1] Title figure inspired from CERN
http://press.web.cern.ch/press-releases/2015/07/cerns-lhcb-experiment-reports-observation-exotic-pentaquark-particles.

[2] S. Weinberg *A Model of Leptons* Phys. Rev. Lett **19**, 1264 (1967).

[3] A. Salam *Weak and Electromagnetic Interactions*, Conf. Proc. C 680519, 367 (1968).

[4] S. L. Glashow *Partial-symmetries of weak interactions*, Nucl. Phys. **22**, 579 (1961).

[5] P.W. Higgs *Broken Symmetries and the Masses of Gauge Bosons*, Phys. Lett. **12**, 132 (1964).

[6] K. A. Olive et al (Particle Data Group), Chin. Phys. C, **38**, 090001 (2014) and 2015 update.

[7] X. Ji *Quarks, Nuclei, and the Cosmos: A Modern Indroduction to Nuclear Physics* Lecture Notes on Phys 741
http://physics.umd.edu/courses/Phys741/xji/lecture_notes.htm.

[8] M. E. Peskin, D. V. Schroeder *An introduction to quantum field theory* (Westview Press, 1995).

[9] H. Yukawa *On the Interaction of Elementary Particles*, PTP, 17, 48.

[10] W. Weise *The QCD vacuum and its hadronic excitations*, arXiv:nucl-th/0504087v1.

[11] S. Scherer *Introduction to Chiral Perturbation Theory*, arXiv:hep-ph/0210398v1.

[12] Kenneth G. Wilson *Confinement of quarks.* Phys. Rev. **D10** (1974) 2445.

[13] C. Gattringer and C. B. Lang *Quantum Chromodynamics on the Lattice.* Springer, Berlin Heidelberg 2010.

[14] H. Wittig *QCD on the Lattice.* Landolt-Börnstein, New Series I/21A.

[15] *QUARK MODEL* (Particle Data Group), Revised August 2013 by C. Amsler (University of Bern), T. DeGrand (University of Colorado, Boulder), and B. Krusche (University of Basel).

[16] R. Alkofer, J. Greensite *Quark Confinement: The Hard Problem of Hadron Physics*, arXiv:hep-ph/0610365v2.

[17] D. J. Gross, F.Wilczek *Ultraviolet Behaviour of Non-Abelian Gauge Theories*, Phy.Rev.Let. 30 (1973) 1343–1346.

[18] B. Z. Kopeliovich, A. H. Rezaein *Applied High Energy QCD*, arXiv:0811.2024v2.

[19] K. Symanzik, *Continuum Limit and Improved Action in Lattice Theories*, Nucl.Phys. B226, 187 (1983).

[20] B. Sheikholeslami and R. Wohlert *Improved continuum limit lattice action for QCD with wilson fermions*
doi:10.1016/0550-3213(85)90002-1

[21] D. Djunkanovic, T. Harris, P. Junnarkar *et. al Nucleon electromagnetic form factors and axial charge from CLS $N_f$=2+1 ensembles* arXiv:1511.07481v1 (2015).

[22] M. Lüscher und S. Schäfer *Lattice QCD without topology barriers*
arXiv:1105.4749v1 (2014).

[23] M. Lüscher und S. Schäfer *Implementation of the lattice Dirac operator* 2012, revised November 2013
http://luscher.web.cern.ch/luscher/openQCD/.

[24] http://luscher.web.cern.ch/luscher/openQCD/.

[25] S. Capitani et al. *Scale setting via the* Ω *baryon mass*
arXiv:1110.6365v1.

[26] V. Gülpers *Hadronic Correlation Functions with Quark-disconnected Contributions in Lattice QCD* Ph.D thesis Johannes Gutenberg University of Mainz (2015).

[27] S. Güsken *A Study of smearing techniques for hadron correlation functions* Nuc. Phys. Proc. Suppl. **17**, 36-364 (1990).

[28] B. Jaeger *Hadronic matrix element in lattice QCD* Ph.D thesis Johannes Gutenberg University of Mainz (2014).

[29] Jacob Finkenrath , Francesco Knechtli , Björn Leder *One flavor mass reweighting in lattice QCD*
arXiv:1306.3962 (2014).

[30] J. Beringer et al. (Particle Data Group), Phys. Rev. **D86**, 010001 (2012)
http://pdg.lbl.gov.

[31] Robert G. Edwards *QDP++ Data Parallel Interface for QCD* Version 1.24.1 (2007).

[32] D. B. Lichtenberg, W.Namgung, E.Predazzi and J.G.Wills *Baryon Masses in a Relativistic Quark-Diquark Model* Phys.Rev.Let 48.1653.

[33] Stefan Scherer ( Group theory I and II) Lecture notes, Johannes Gutenberg University.

[34] A. Zee *Quantum Field Theory in a Nutshell* (Princeton University Press).

[35] G. Martinelli and C. T. Sachrajda *A Lattice Study of Nucleon. Structure* Nucl.Phys. **B316** (1989) 355.

[36] D. B. Renner *et.al Calculation of the nucleon axial charge in lattice QCD* Journal of Physics: Conference Series **46** (2006) 152-156.

[37] T. Streuer *Simulation der Quantenchromodynamik mit Overlap-Fermionen* Dissertation, Freie Universität Berlin (2005).

[38] R. L. Jaffe *Polarized Λ's in the current fragmentation region* Phys. Rev. **D54** (1996) 6581

[39] N. Cabibbo *Unitary symmetry and leptonic decays* Phys. Rev. Lett **10** (1963) 531.

[40] P. Renton *Electroweak interactions: An introduction to the physics of quarks & leptons* Cambridge Unversity Press 1990.

[41] K. Dannbom and D.O. Riska *The axial current of the hyperons in the topological soliton model* Nuc. Phys. **A548** (1992) 669-680.

[42] Harvey B. Meyer *Calculation of nucleon form factor* Institut für Kernphysik, Johannes Gutenberg Universität Mainz, (update 24.02.2014).

[43] T. Ledwig, J. Martin Camalich, L. S. Geng and M. J.Vicente Vacas: arxiv.org/abs/1405.5456v1

[44] B. Knippschild *Baryons in the chiral regime* Ph.D thesis Johannes Gutenberg University of Mainz (2011).

[45] S. Capitani et al. *Nucleon axial charge in lattice QCD with controlled errors* PRD **86**, 074502 (2012).

[46] B. Efron *Bootstrap methods: Another look at the Jackknife* http://projecteuclid.org/download/pdf_1/euclid.aos/1176344552.

[47] A. McIntosh *The Jackknife Estimation Method* http://people.bu.edu/aimcinto/.

[48] Stephen So *Why is the sample variance a biased estimator?* Griffith School of Engineering, Griffith University, Brisbane, QLD, Australia, 4111, September 11, 2008 http://www.marcovicentini.it/wp-content/uploads/2014/07/La-correlazione-di-Bessel.pdf.

[49] Carleton DeTar, http://www.physics.utah.edu/ detar/phycs6730/.

[50] J. David Irwin *The Industrial Elctronics Handbook*, May 9, 1997 by CRC Press

[51] M. G. Endres et al. *Noise, Sign Problems, and Statistics* PRL **107**, 201601 (2011), 10.1103/PhysRevLett.107.201601.

[52] D. Griffiths *Introduction to Elementary Particles* Second, Revised Edition.

[53] F. Fucito, E. Marinari, G. Parisi, C.Rebbi *A proposal for monte carlo simulations of fermionic systems* Nuc.Phys. B180[FS2] (1981) 369-377.

[54] C. Alexandrou, R. Baron, M. Brinet, J. Carbonell, V. Drach et al., *Nucleon form factors with dynamical twisted mass fermions*, http://arxiv.org/abs/0811.0724.

[55] J. Bulava, M. D. Norte, J. Heitger, C. Wittemeier *Non-perturbative improvement and renormalization of the axial current in $N_f$=3 lattice QCD* http://arxiv.org/abs/1502.07773.

[56] S. Sint, P. Weisz *Further results on O(a) improved lattice QCD to one-loop order of perturbation theory* http://arxiv.org/abs/hep-lat/9704001

[57] M. Bruno, D. Djukanovic, G. P. Engel, A. Francis, G. Herdoiza, et al. *Simulation of QCD with $Nf = 2 + 1$ flavors of non-perturbatively improved Wilson fermions* JHEP 1502 (2015) 043, arXiv:1411.3982.

[58] V. Bernard, N. Kaiser, U. Meißner *Critical analysis of baryon masses and sigma-terms in heavy baryon chiral pertubation theory* http://arxiv.org/abs/hep-ph/9303311.

[59] W. Söldner *Lattice QCD with 2+1 flavors and open boundaries: First results of the baryon spectrum* arXiv:1502.05481v2.

[60] W. Bietenholz, V. Bornyakov, M. Göckeler et al. *Flavor blindess and patterns of flavor symmetry breaking in lattice simulations of up, down, and strange quarks* Phys. Rev. D **84**, 054509 (2011).

[61] P. C. Bruns, L.Greil and A.Schäfer *Chiral extrapolation of mass ratios* http://arxiv.org/abs/1209.0980.

[62] M. Bruno, D. Djukaovic, G. P. Engel et al. *Simulation of QCD with $N_f$=2+1 flavors of non-perturbatively improved Wilson fermions* arXiv:1411.3982.

[63] D. Guadagnoli, V. Lubicz, M. Papinutto, S. Simula *First Lattice QCD Study of the $\Sigma^- \longrightarrow n$ Axial and Vector Form Factors with SU(3) Breaking Corrections* arXiv:hep-ph/0606181v2.